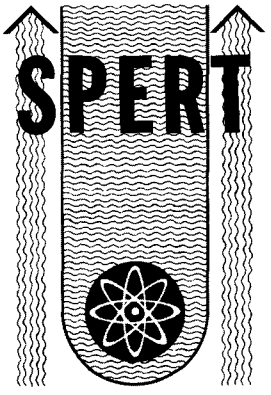

IDO-16884
AEC Research and Development Report
Reactor Technology
TID-4500 (30th Ed.)
Issued: June 1964

TRANSIENT TEMPERATURE DISTRIBUTIONS IN THE SPERT I D-12/25 FUEL PLATES DURING SHORT-PERIOD POWER EXCURSIONS

by

J. E. Houghtaling
Alain Sola (EURATOM)
A. H. Spano

PHILLIPS
PETROLEUM
COMPANY

Atomic Energy Division
Contract AT(10-1)-205
Idaho Operations Office
U. S. ATOMIC ENERGY COMMISSION

DISCLAIMER

ABSTRACT

This report presents the results of experimental measurements and calculations of the transient fuel plate temperatures obtained in the short-period power excursion tests of the Spert I plate-type destructive test program. In this program, step-initiated, self-limiting transients, with reactor periods in the range from 1.3 sec to 3.2 msec, were performed on a water-moderated, highly enriched U-Al alloy, plate-type core. In the final 3.2-msec-period test, a large amplitude pressure burst was suddenly generated several msec after the nuclear excursion had effectively terminated, resulting in large scale destruction of the core. Transient fuel plate surface temperature data were obtained during the tests using small-mass, fast-response, chromel-alumel thermocouples. These data have been used as input in computer calculations of the transient temperature distributions in the fuel plates. For the 3.2-msec-period destructive test, the calculational results indicate that the fuel plate meat temperature at the core hot spot reached a maximum value of approximately 1400°C during the excursion, decreasing thereafter to a value of about 1000°C at the time the core was violently destroyed. Based on these calculations approximately one-third of the fuel plate volume in the core had reached the melting point at the time of core destruction. The fuel plate temperatures achieved during the destructive test do not appear to be sufficiently high to make an aluminum-water chemical reaction a reasonable cause of the large, sudden pressure burst which was observed. A more likely mechanism, consistent with the analytical results showing that a sizeable volume of the core was in a molten and physically weakened condition at the time of the pressure pulse, involves the self propagating effect of rapid fuel plate fragmentation giving rise to high heat transfer rates to the water with the consequent generation of large steam pressures.

Errata for IDO-16884

TRANSIENT TEMPERATURE DISTRIBUTIONS IN THE SPERT I
D-12/25 FUEL PLATES DURING SHORT-PERIOD POWER EXCURSIONS

Page 2, Section 2.1, line 3 - substitute "... 0.0005 in. ..." for
".. 0.005 in. ..".

Page 32, Ref. 2 - the report number is IDO-16883, not 16884.

TRANSIENT TEMPERATURE DISTRIBUTIONS IN THE SPERT I D-12/25 FUEL PLATES DURING SHORT-PERIOD POWER EXCURSIONS

CONTENTS

FIGURES

TABLES

I. INTRODUCTION

The Spert I destructive test of a plate-type core in November 1962 constituted the first of such tests conducted at Spert as part of an overall program to investigate the destructive consequences of a reactivity accident for a given class of cores. The destructive test program is designed to provide information on questions relating to reactor kinetics and shutdown behavior; the initiation and nature of explosive reactions in reactor accidents; the mechanical effect of explosions on reactor environs; and the extent of radiation exposure, fission product release, etc, resulting from a destructive burst.

In the destructive test program [1, 2] of the Spert I aluminum-clad, plate-type core (designated the D Core), a series of step-initiated power excursion tests was performed, with asymptotic reactor periods in the range from about 1.3 sec to 3.2 msec. For periods as short as 6 msec, damage was restricted primarily to fuel plate distortion, and, as observed in some fuel plates, to temporary loss of tensile strength. Damage effects in a 5-msec-period test included not only fuel plate warping, but also (in the central six-plate fuel assembly of the core) a melting and fusing together of fuel plates. In a 4.6-msec-period test, fuel plate damage effects, while similar in kind to those of the 5-msec-period test, were more extensive, with melting obtained in 52 of the 270 fuel plates in the core, many of them being fused together. In each of these tests, new fuel assemblies were installed to replace those damaged in the previous test.

The test program culminated in a successful destructive test on November 5, 1962. The excursion, self-limiting in character with predictable burst parameters, gave rise to a violently destructive pressure pulse approximately 15 msec after peak power. The results of this test are described in detail in Ref. 2.

To help understand the cause of the destructive pressure pulse, information on the fuel plate temperature behavior during the excursion is of highest importance. Fuel plate temperature data were obtained using (a) fast-response cladding surface thermocouples, (b) thermocouples embedded in the meat of the fuel plate, and (c) thermocouples placed in small stainless steel containers (fuel cells) containing small amounts of the uranium-aluminum alloy material used in the fuel plates. The most useful data obtained are those of the cladding surface temperature, which are reliable to temperatures up to about 400°C, above which some uncertainty in the cladding temperature data appears to be indicated. The cladding surface temperature data were used as a basis for fuel plate transient temperature distribution calculations.

The body of the report discusses the thermocouple instrumentation used, the experimental and calculational fuel plate temperature information obtained for several of the short-period tests of the program, and the probable physical state of the core at the time of the 3.2-msec-period destructive pressure pulse and the implications thereof.

II. DESCRIPTION

1. CORE

The Spert I destructive core (D Core) was comprised of 25 fuel assemblies mounted in a 5 x 5 array in a rectangular grid structure, as shown in Fig. 1. Four symmetrically-placed, gang-operated control rod assemblies, each consisting of a pair of poison blades with aluminum followers, provided reactor control. An additional, centrally-located transient rod assembly consisting of two aluminum blades with poison follower blades was used to initiate experimental reactor transients. A cross sectional view of the core, shown in Fig. 2, indicates the relative positions of the fuel, transient rod, and control rods. The core was mounted in the 10-ft-diameter, open tank facility at Spert I, which has no provision for forced coolant circulation.

Each standard fuel assembly contained 12 removable fuel plates. The four control-rod and one transient-rod fuel assemblies each contained only six removable fuel plates, the remaining six fuel plate positions being occupied by the two control blades and their housings. Each fuel plate consisted of a 0.020-in.-thick section of highly enriched U-Al alloy fuel meat, clad on each side with a 0.020-in. wall thickness of 6061-aluminum alloy. Overall dimensions of the fuel plate were 0.060 in. thick by 2.704 in. wide by 25-1/8 in. long, and the nominal width of the water channel was 0.179 in. Each plate contained 14 g of U-235.

2. THERMOCOUPLE INSTRUMENTATION

Various fuel plates throughout the core were instrumented with cladding surface thermocouples and with ("buried") thermocouples embedded in the meat of the fuel plate. Figs. 3, 4, and 5 illustrate typical fuel plates instrumented with surface and buried thermocouples.

2.1 Fuel Plate Surface Thermocouples

The surface thermocouples were comprised of 0.010-in.-diameter, nylon-insulated, chromel-alumel wires, the ends of which were stripped of insulation and flattened into thin "wafers" about 0.005 in. thick, which were discharge-welded to the fuel plate surface. As shown in Fig. 5, the method of attaching the wire to the plate involved the use of a cross wire connected to the main wire, such that, with the three wire ends welded to the plate surface, a multiple contact point could be obtained. This multiple contact provided a measure of the average temperature of the three junctions, reducing the importance of temperature variations on the surface that could result from fuel inhomogeneities or localized boiling. The multiple junction also reduced the probability of overall thermocouple failure and the loss of all information.

2.2 Buried Thermocouples

Thermocouples embedded in the fuel plate were comprised of 0.005-in.-diameter, chromel-alumel, nylon-insulated wires, with 0.005-in.-diameter,

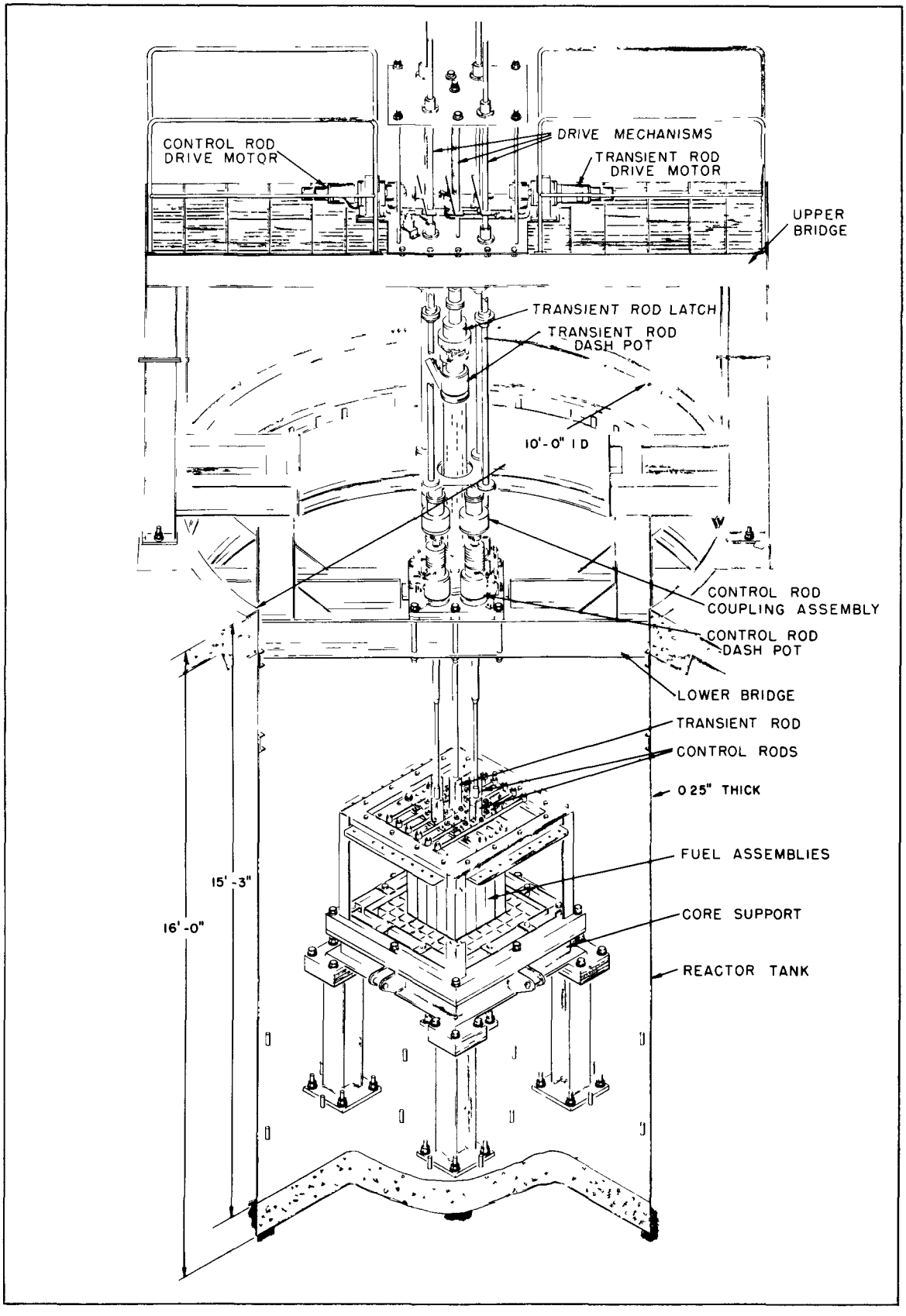

Fig. 1 Cutaway view of the Spert I reactor.

cross arms welded near the ends. The ends of the cross arms were embedded in the fuel plate to a depth of approximately 0.030 in., near the center of the plate. The wires were laid in a thin groove cut into the plate to the desired depth, with the lip of the cut then peened back over the wires, as shown in Fig. 5. It was expected that in a severe power excursion the buried thermocouples would persist longer than the cladding surface thermocouples before high temperature failure occurred. This behavior is indicated in the temperature traces obtained from a cladding surface thermocouple and from a buried thermocouple during the 4.6-msec-period test (Fig. 8, page 11).

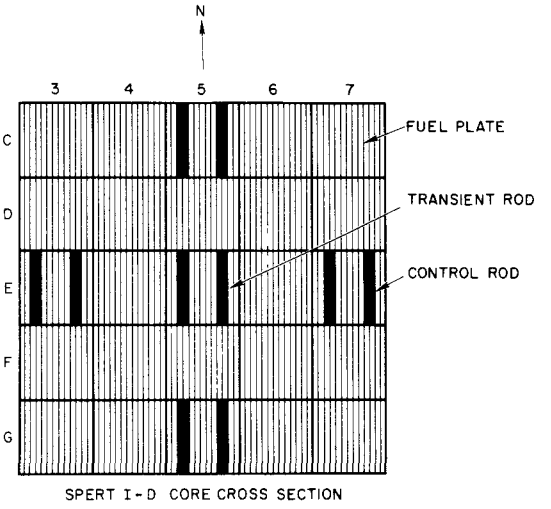

Fig. 2 Cross section through the Spert I-D core.

2.3 Fuel Cell Thermocouples

In an attempt to obtain a measure of the actual fuel temperature in the core at times after fuel plate melting had taken place, two special capsules were constructed and installed in the core prior to the final (3.2-msec-period) destructive test. Each capsule was made from a flattened stainless steel tube (3/16 in. diameter x 3/8 in. long x 0.020-in. wall thickness), welded closed at each end. The capsule contained two 0.020-in.-thick pieces of the uranium-aluminum meat alloy used in the fuel plates, with a W/W-Rh thermocouple junction placed between the two small sections of meat. The thermocouples were then placed in a small-diameter stainless steel tube which penetrated the welded top end of the capsule. The capsule was then heated in an oven to a temperature exceeding the melting point of the U-Al alloy to ensure good contact between the meat and the thermocouple junction. A fuel capsule mounted on a fuel plate is illustrated in Fig. 6.

2.4 Signal Conditioning

Thermocouple leads were connected through a reference junction to a low-level DC amplifier, followed by a voltage-to-current amplifier. The signals were then transmitted 3000 ft to a recording oscillograph located in the reactor control building. The frequency response of the system was limited by that of the oscillograph recorder, which is linear up to 3 kc, but reduced by 3 dB at 5 kc.

2.5 Designation of Thermocouple Location in the Core

Fuel assembly lattice positions in the D Core were specified by a letter and number (Fig. 2). Within a fuel assembly, the fuel plates were numbered from west to east (left to right in Fig. 2) with the east or west side of the plate designated by E or W, respectively. In addition, the vertical distance in inches of any point from the center of the core was specified to be positive for points above the center plane of the core or negative for points below the center plane. Thus, the designations of the surface and buried thermocouples (specified by the letter B) located at the center of the core are, respectively, E5(7W)0 and E 5 (7W)0B.

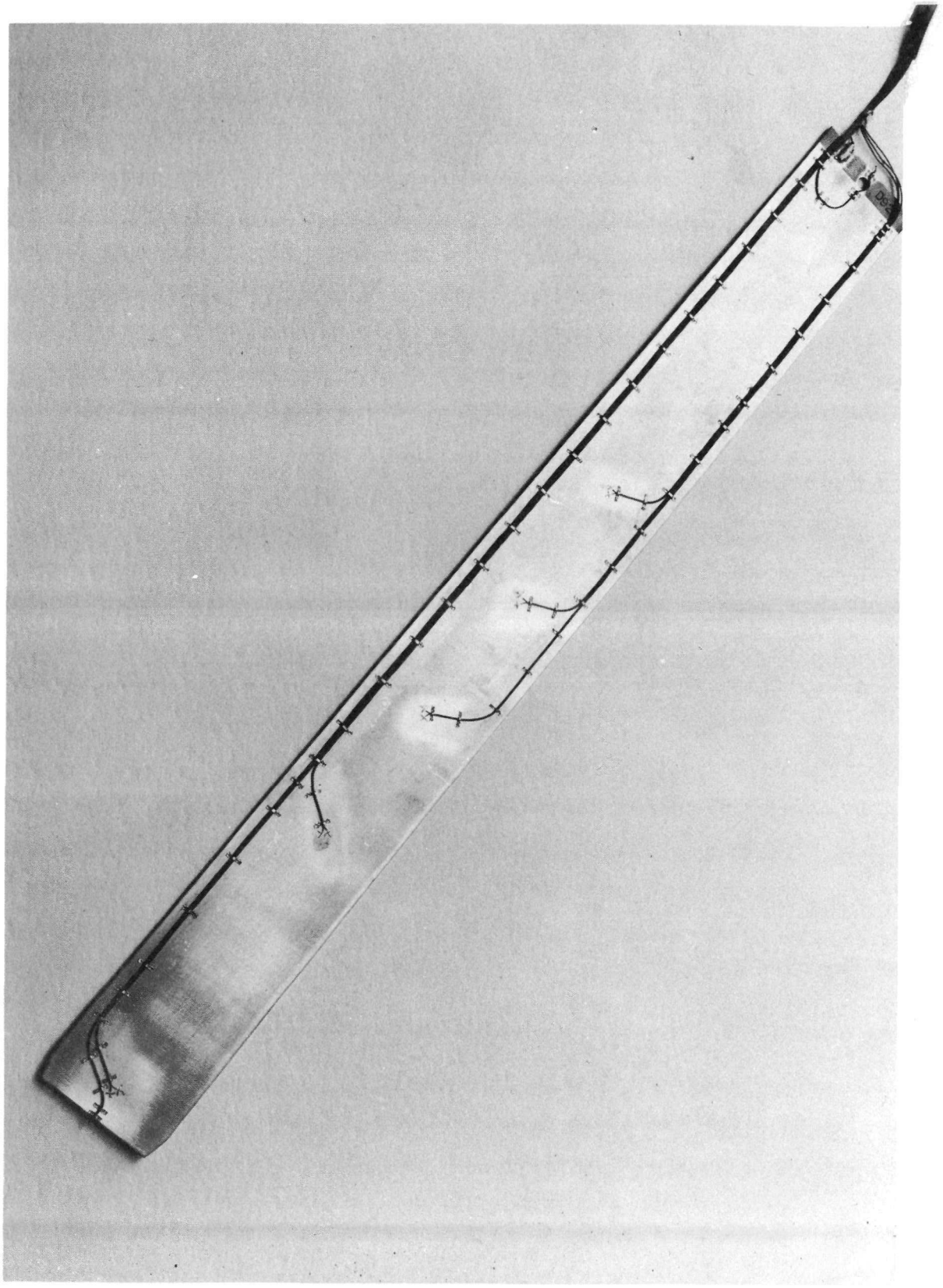

Fig. 3 Fuel plate instrumented with surface thermocouples.

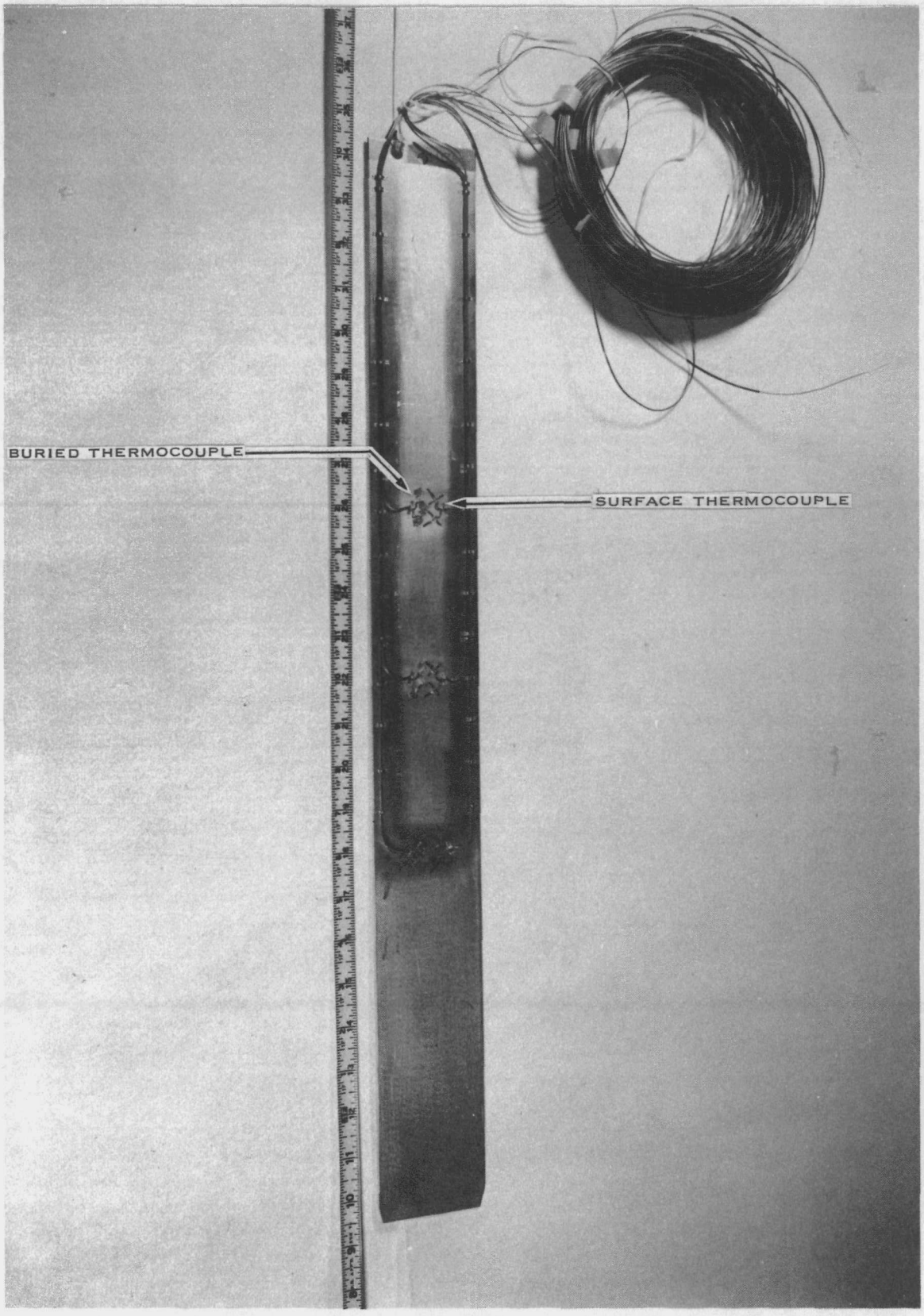

Fig. 4 Fuel plate instrumented with surface thermocouples and buried thermocouples.

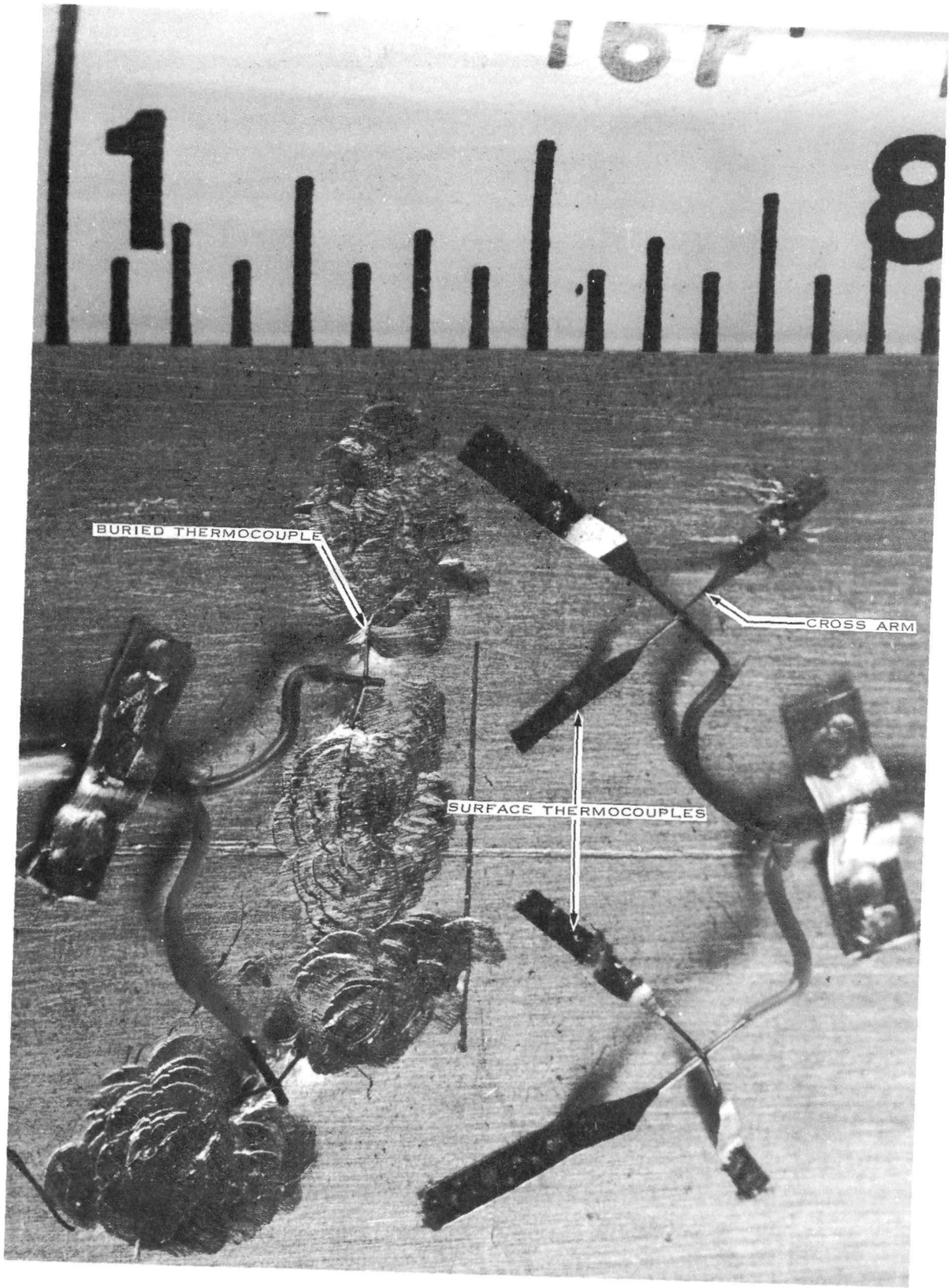

Fig. 5 Detail of typical fuel plate showing surface thermocouple junctions connected in parallel and buried thermocouple junctions peened into the plate.

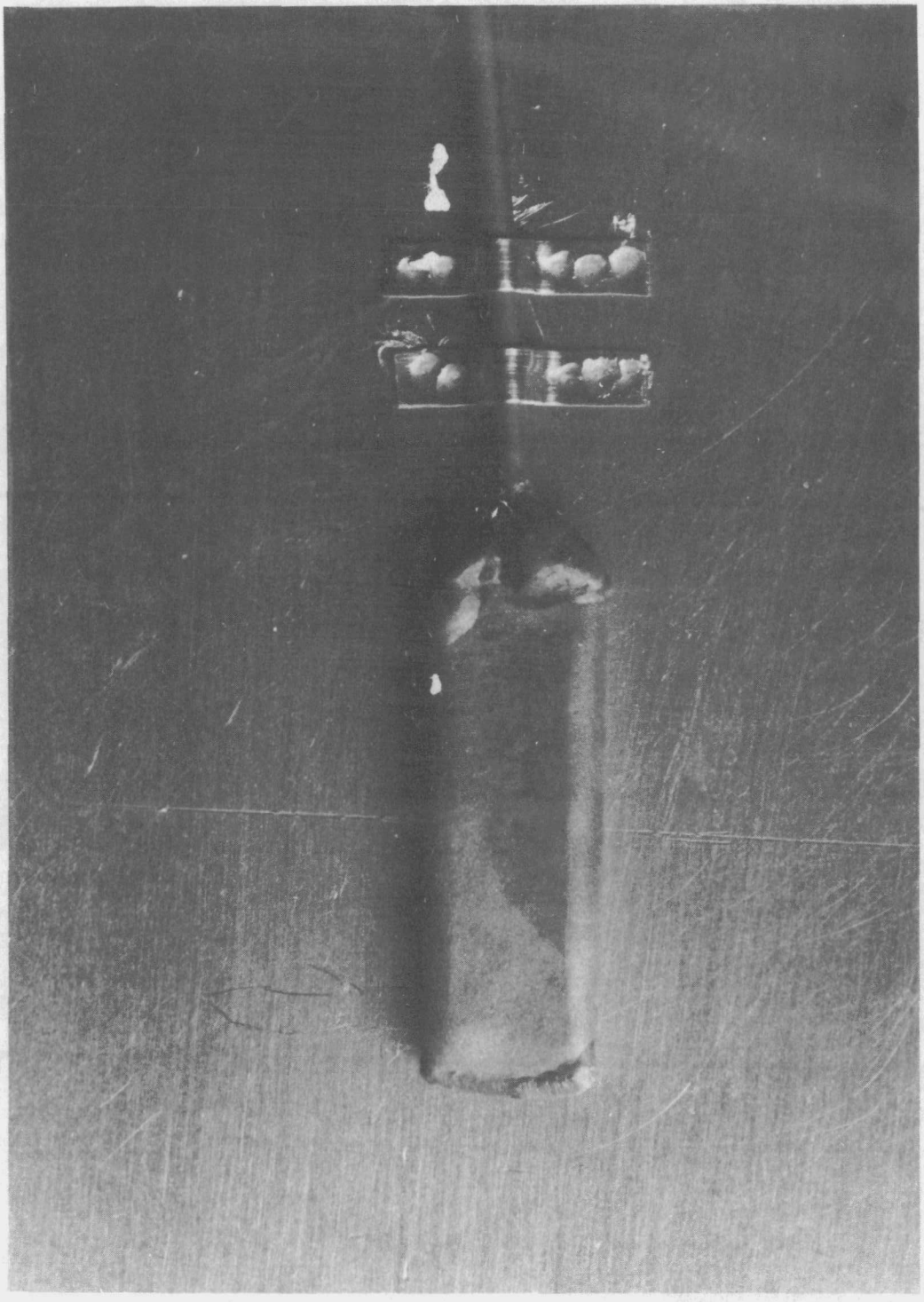

Fig. 6 Fuel capsule mounted on a fuel plate.

III. EXPERIMENTAL TEMPERATURE MEASUREMENTS

1. POWER EXCURSION TEST SERIES

A series of 54 step-initiated, self-limiting power excursion tests was carried out in the Spert I-D core, with initial asymptotic reactor periods in the range from 1310 to 3.2 msec. The following burst parameters are summarized in Table I [3]: τ_o, reactor period; α_o, reciprocal period; Δk_o, step reactivity insertion; $\phi(t_m)$, peak power; $E(t_m)$, energy release to time of peak power; E_T, total burst energy; $\theta(tm)$, fuel plate temperature at E5 (7W)-3 at peak power; and θmax, maximum fuel plate temperature at E5 (7W)-3. The thermocouple position E5 (7W)-3 represented the approximate flux peaking point in the core during the long-period tests (roughly, 50 msec or longer). For the shorter-period tests, corresponding to higher control rod positions, the flux peaking point in the core was more nearly represented by the slightly higher thermocouple position of E5 (7W)0.

2. TRANSIENT FUEL PLATE TEMPERATURE DATA

Transient cladding surface temperature data obtained at the core hot spot, E5 (7W)0, during the five shortest-period tests of the transient series are shown in Fig. 7. The initial temperature for each trace is approximately 20°C. The temporary halt in temperature rise that is generally evident in the traces in the temperature range above the saturation point and below 200°C is believed to be the result of high heat transfer rates obtained momentarily during the nucleate boiling phase.

In each of the tests with reactor periods less than 6 msec, the surface thermocouple in Fig. 7 failed at a temperature below the Al-6061 cladding melting range of about 620 - 650°C. This failure is attributed to the differential thermal expansion between the meat and cladding, and/or the generation of cracks by hot short cracking inside the fuel plate at high temperatures. Fairly large fuel plate cracks were detected in post-test metallurgical examinations of various fuel plates for the transient tests with periods shorter than about 6 msec [4], in which the maximum cladding surface temperatures at the core hot spot exceeded 550°C.

Figs. 8 and 9 show buried and cladding surface temperature traces from the 4.6- and 3.2-msec-period tests, respectively. The two transducers of Fig. 8 were on opposite sides of the central coolant channel of the E6 fuel assembly, which is adjacent to the central fuel assembly of the core (see Fig. 2). The two transducers referred to in Fig. 9 were about 1/2 in. apart on the same plate of the central fuel assembly (E5). For reactor periods below about 20 msec, the buried thermocouples consistently indicated temperatures 10 to 25 percent higher than those given by surface thermocouples, but considerably lower than the corresponding meat temperatures indicated by the fuel capsule thermocouples. In Fig. 8, an example is indicated of a cladding surface thermocouple that failed early, at a temperature of roughly 100°C below the melting point of the cladding material.

TABLE I

TRANSIENT TEST DATA SUMMARY

Run No	τ_o (msec)	ω_o (sec^{-1})	Δk_o ($)	$\phi(t_m)$ (Mw)	$E(t_m)$ (Mw-sec)	E_T (Mw-sec)	$\theta(t_m)$* (°C)	θ_{max}* (°C)	Date (1962)
									April
1	930	1 08	0 80	0 67	1 84	(d)	65(a)	89(a)	5
2	640	1 56	0 85	0 98	1 76	(d)	66	95	10
3	355	2 82	0 92	1 50	1 47	(d)	61	98	10
4	163	6 14	0 99	3 25	1 13	(d)	60	104 105(a)	10
5	98	10 2	1 05	6 60	1 34	(d)	73	110	11
6	65	15 4	1 10	14 2	1 68	(d)	92 93(a)	115	11
7	47	21 3	1 16	27 5	2 25	3 95	110	117	11
8	34	29 4	1 23	50 0	2 90	4 90	122	124	11
9	25	40 0	1 32	87 0	3 20	4 90	130	132	12
10	19	53	1 42	141	4 05	5 85	145	150	12
11	14 5	69	1 56	210	4 10	5 80	156 164(a)	165	12
12	12 1	83	1 67	290	4 60	6 45	166	180	12
13	9 8	102	1 80	380	5 15	7 55	180	227	12
14	9 5	105	1 85	430	5 70	7 85	188	255	13
15	8 2	122	1 99	530	5 85	8 55	181	315	16
16	7 2	139	2 13	630	6 00	9 32	181	360 375(a)	17
17	6 9	145	2 18	690	6 45	10 2	174 203(a)	400	17
18	6 8	147	2 20	685	6 05	10 00	188 198(a)	420	19
19	6 4	156	2 27	745	6 60	10 5	176 198(a)	455	19
									May
22	880	1 14	0 81	0 98	(d)	(d)	54(a)	94(a)	10
23	19 3	52	1 42	120	3 40	4 70	125	132	10
24	9 0	111	1 90	395	4 70	7 10	157	300	10
25	7 5	133	2 08	555	5 55	8 80	158	355	11
26	6 0	167	2 36	890	7 20	13 2	185 210(a)	545 560(a)	11
27	8 1	124	2 00	505	5 45	9 20	177	325	16
28	5 0	200	2 63	1130	8 35	17 5	320	585	18
									June
29	49 5	20 2	1 13	19 1	1 84	3 20	125(b)	129(b)	6
30	7 6	132	2 03	510	5 20	9 40	172 250(b)	400 465(b)	6
31	6 9	145	2 14	620	6 40	10 9	190 290(b)	440 490(b)	8
32	4 6	218	2 72	1270	8 90	19 0	240 420(b)	570 680(b)	11
									July
33	380	1 14	0 81	0 76	1 79	(d)	64(b)	94(b)	23
34	118	8 48	1 03	4 50	1 00	(d)	59 67(b)	102 109(b)	24
35	21 7	46 1	1 37	107	3 40	5 05	125 149(b)	128 155(b)	24
36	8 9	112	1 91	460	5 05	7 65	151 230(b)	242 350(b)	26
37	880	1 14	0 81	0 78	2 21	(d)	69(b)	87(b)	26
38	112	8 93	1 03	5 05	1 18	(d)	63 68(b)	99 117(b)	26
39	22 4	45 8	1 35	105	3 60	5 40	120 146(b)	124 154(b)	27
40	8 7	115	1 93	470	5 25	8 20	167 216(b)	234 305(b)	27
41	6 8	147	2 20	635	5 75	9 20	232(b)	355(b)	30
42	6 9	145	2 18	640	6 00	9 70	156 246(b)	340 430(b)	31
									August
43	6 9	145	2 18	660	6 35	10 4	160 243(b)	340 440(b)	1
44	6 9	145	2 18	665	6 60	10 4	161 250(b)	325 440(b)	2
									October
46	1310	0 76	0 75	0 39	1 49	(d)	65(b)	80(b)	18
47	243	4 12	0 95	1 43	0 91	(d)	61(a)	93(a)	19
48	140	7 14	1 02	3 80	0 94	(d)	62(a)	112(a)	22
49	21 1	47 4	1 38	110	3 60	5 40	148(b)	153(b) 220(c)	22
50	9 6	104	1 85	350	5 00	7 15	195(b)	232(b) 350(c)	22
51	7 0	1 3	2 16	620	6 45	10 2	223(b)	305(b) 455(c)	22
52	9 6	104	1 85	380	5 10	7 25	208(b)	229(b) 360(c)	24
53	9 7	103	1 84	360	5 05	7 45	204(b)	234(b) 350(c)	24
									November
54	3 2	313	3 55	2250	13 8	30 7	430(b)	615(b) 1230(c)	5

* Surface temperature measured at E5 (7W)-3
(a) Highest surface temperature measured at a position other than E5 (7W)-3
(b) Temperature measured using buried thermocouple.
(c) Maximum temperature measured using special fuel cell thermocouple
(d) Total energy undefined due to absence at long periods of a distinct power cutoff

Fig. 10 shows, for the 3.2-msec-destructive test, fuel plate meat temperatures (as indicated by buried thermocouples) in the horizontal plane 8 in. above the center plane of the core, at the onset of the destructive pressure pulse, about 15 msec after peak power. Additional buried thermocouple temperatures at the time of the pressure burst at several points in the horizontal plane 4 in. below the core center are listed in Table II. Although the measured buried thermocouple temperatures in the +8- and -4-in. planes are all below the melting temperature of aluminum, considerations of the temperature distributions in the fuel plate (discussed later in this report) indicate that an appreciable portion of the core was in the molten state at the time of the pressure burst.

Fig. 11 presents transient test data on the maximum fuel plate surface temperature obtained at position E5(7W)-3 and data on the total burst energy as a function of the reciprocal period. The break in the maximum surface

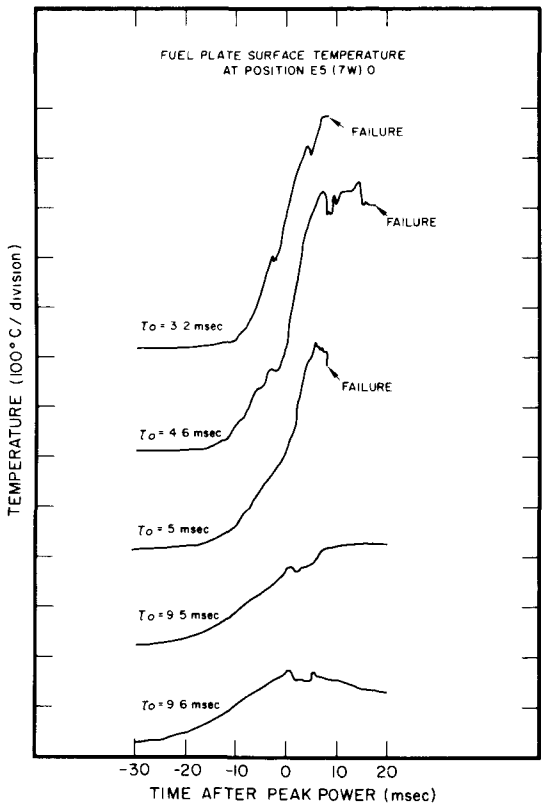

Fig. 7 Transient fuel plate surface temperature data at position E5(7W)0.

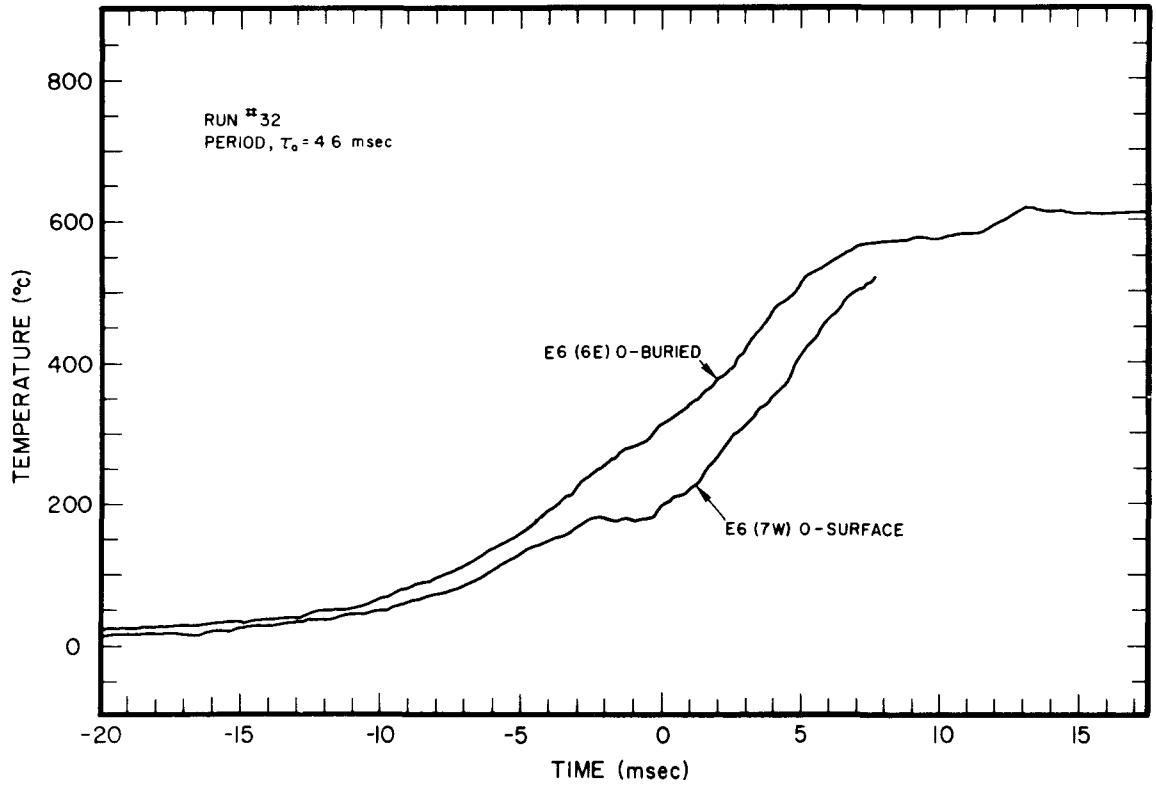

Fig. 8 Transient temperature data obtained with buried and surface thermocouples during the 4.6-msec-period test.

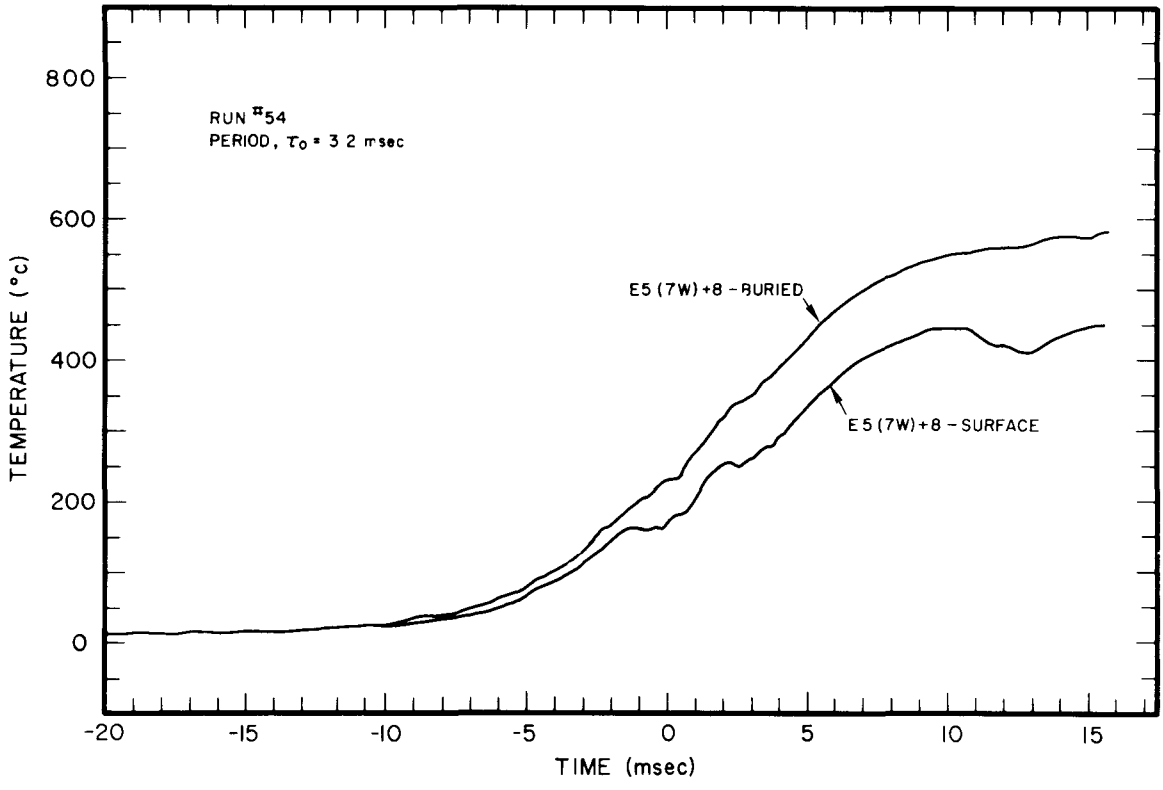

Fig. 9 Transient temperature data obtained with buried and surface thermocouples during the 3.2-msec-period destructive test.

temperature curve occurring in the vicinity of the melting point of aluminum can be understood in terms of a reduction in heat transfer from the meat to the cladding surface as a result of the loss of energy in heat of fusion as the meat melts, and as a result, perhaps, of hot short cracking in the cladding. The upper, dashed portion of the temperature curve in Fig. 11 represents the estimated probable peak temperatures obtained when the melting point of aluminum has been reached. The plateau takes into account the relative constancy of the temperature during the melting process in the plate. Beyond the plateau, the maximum surface temperature increases in proportion to the energy absorbed by the plate after completion of melting.

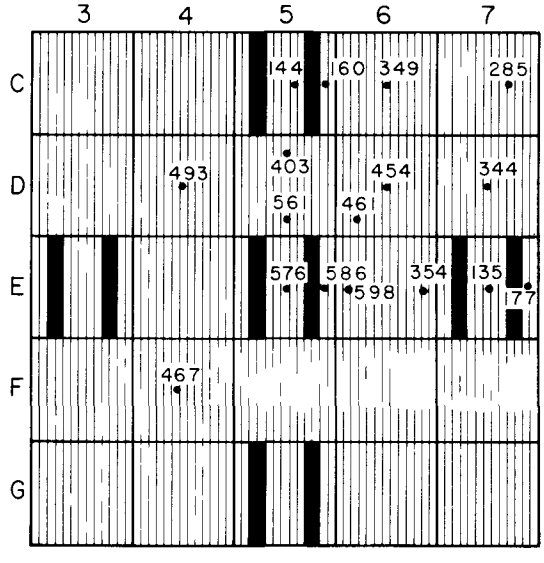

Fig. 10 Fuel plate temperatures indicated by the buried thermocouples in the +8-in. plane at the time of core destruction.

Fig. 12 is a summary plot of the maximum temperatures measured during an excursion as a function of the total burst energy released. The data were obtained from surface and buried thermocouples at E5(7W)-3 and other nearby positions, and from a fuel capsule thermocouple located at E6(3W)-4 (at a point where the power density is approximately 15 percent below the peak power density in the core). The solid curve is calculated, and represents the maximum, isothermal temperature obtained in an insulated fuel plate at the core hot spot as a function of the total energy released in a burst. As seen in Fig. 12, the experimental data fall below the calculated curve, except for the two points obtained during the 4.6- and 3.2-msec-period tests. The fact that these two meat temperature data are above the isothermal adiabatic temperature curve in contrast to corresponding thermocouple data lying below the curve in the longer period (lower energy) region may be understood in terms of the greater fuel plate temperature gradients achieved in the shorter-period tests. In the temperature region below the melting point, the indicated slope of the distribution of experimental points is seen to be relatively steeper than the slope of the adiabatic curve, an effect which can be interpreted in terms of the increased thermal insulation of the fuel plates provided by film boiling as the reactor period is reduced.

The fuel capsule thermocouple data in Fig. 12 are not directly comparable with the fuel plate thermocouple data, but because the capsule fuel is relatively well insulated in comparison with a fuel plate, the capsule data are useful in providing a rough measure of the maximum meat temperatures achieved in the core during an excursion. In the temperature region below the melting point, the capsule temperature data are seen to be approximately proportional to the calculated adiabatic temperatures. For the destructive test, the maximum measured capsule temperature at E6(3W)-4

TABLE II

BURIED THERMOCOUPLE TEMPERATURE DATA AT TIME OF DESTRUCTIVE PRESSURE BURST

Thermocouple Location	Temperature (°C)
E5 (7W) - 4B	620
D6 (7W) - 4B	601
D5 (7W) - 4B	578
E6 (2W) - 4B	597
C7 (9E) - 4B	576

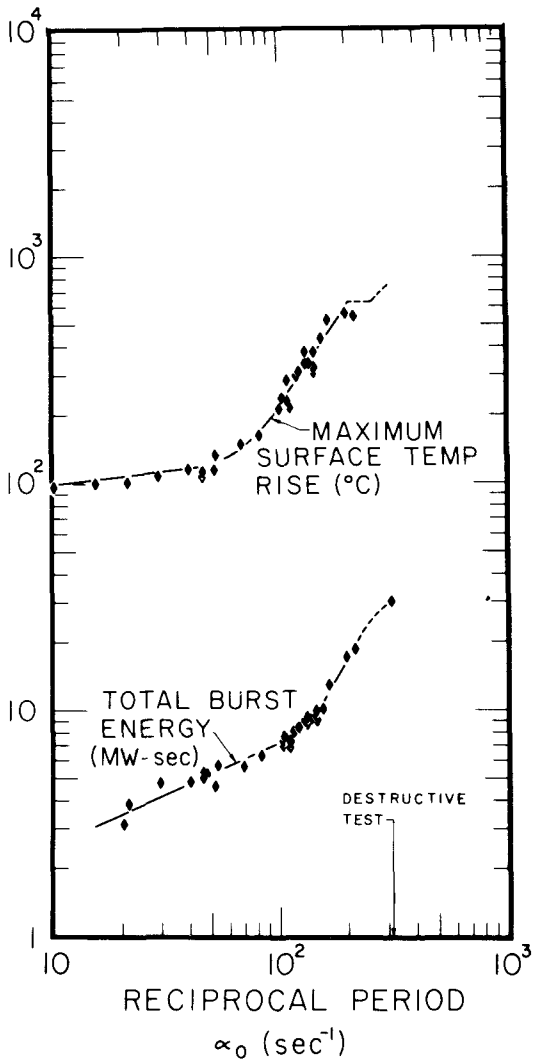

Fig. 11 Maximum fuel plate surface temperature and total burst energy versus reciprocal period.

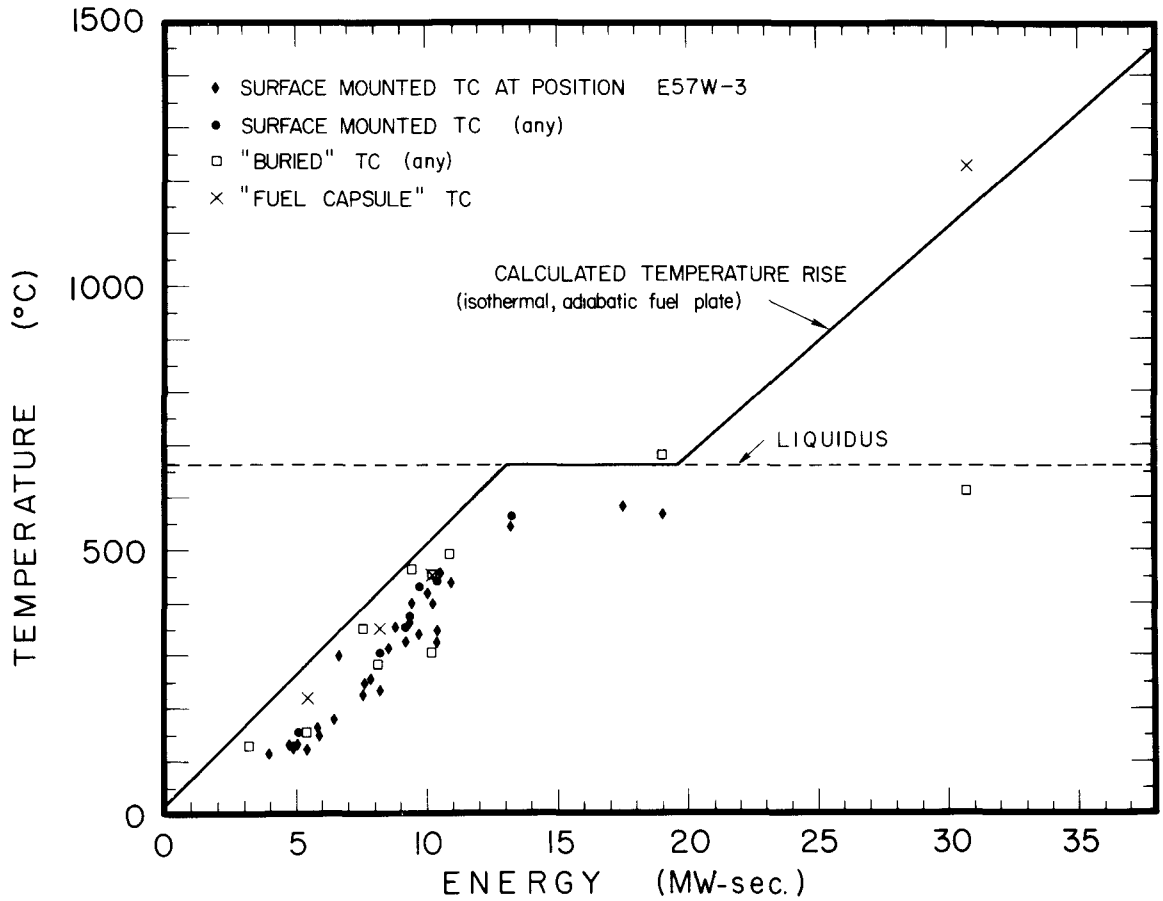

Fig. 12 Maximum temperatures as a function of total burst energy.

was approximately 1200°C. If normalized to the core hot spot, this value would be increased by roughly 15 percent.

3. ERRORS IN TEMPERATURE MEASUREMENTS

As noted above in connection with Fig. 11, the maximum fuel plate temperature data were not extrapolable in the very short-period region (less than 5 msec) where the fuel plate surface temperature at the core hot spot should have approached or exceeded the melting point. This effect may be due to nonvalidity of the standard chromel/aluminum-aluminum/alumel calibration curve used when the temperature is near the melting point of the aluminum cladding. A static temperature calibration of the chromel-alumel thermocouples used in the D̄ Core yielded a voltage output at 200°C that was approximately four percent lower than that indicated in the standard calibration curve [5], a possible consequence of the alloying of the fuel plate metal during the welding process. The true plate temperature also could have been less than expected for either of the following reasons: first, as a result of the heat storage mechanism involved in the melting process; and, secondly, as a result of cracking in the fuel plate. There is evidence [4] that the boundary between the fuel meat and the cladding could have been separated at a number of points by shearing stresses as the fuel meat approached the melting temperature. The development of such cracks would result in a thermal gap resistance, which could significantly reduce the heat

transfer rate to the cladding and give rise to a lower cladding surface temperature than what might otherwise be expected for the case of no stress cracking in the plate.

When the junction of a thermocouple lies in a temperature gradient, the measured temperature depends both upon the gradient and the thermocouple geometry. The smaller the junction, the better defined is the measured temperature. H. Emmons [6] has shown that the thermocouple voltage output depends upon the shape of the junction, on the ratio of the resistivities of the two metals, and on the location of the attachment of the thermocouple lead wires. For instance, when the metal width is greater than the junction length (ie, a short, wide junction) the temperatures at all points of the junction are about of equal importance in their effect on the overall indicated temperature. On the other hand, for long, narrow junctions, the temperature at the points of the junction nearer to the lead wire connection have more effect on the overall indicated temperature than the more distant junction points. On this basis, the short, wide surface thermocouple junctions used in the present tests would appear to have provided an approximate average value of the temperature at the junction.

It has been noted above that the buried thermocouples indicated higher temperatures than did the surface-welded thermocouples. For several tests with periods below about 21 msec, however, the measured fuel capsule meat temperatures were relatively higher than the corresponding meat temperatures indicated by the buried thermocouples. The results indicate that these buried thermocouples monitored temperatures at undetermined points intermediate between the fuel plate center and the cladding surface. Thus, a quantitative comparison of the measured buried thermocouple temperature data with the results of the calculated meat temperature data (discussed in the following section) cannot be made meaningfully.

In summary, the cladding surface thermocouple data are believed to be reliable up to roughly 400°C. Above this temperature, there is some uncertainty as to how well the measured surface temperature data reflect the actual surface temperature, particularly in the vicinity of the melting point of the aluminum cladding.

IV. CALCULATED FUEL PLATE TEMPERATURE DISTRIBUTIONS

1. CALCULATIONAL METHOD

The transient fuel plate temperature distribution was calculated for several transient tests using the HEAT-1 program [7] to solve the one-dimensional partial differential equation for the diffusion of heat in the fuel plate:

$$\frac{\partial}{\partial t}\left[C(\theta,x)\ \theta(x,t)\right] = \frac{\partial}{\partial x}\left[k(\theta,x)\ \frac{\partial}{\partial x}\ \theta(x,t)\right] + S(x,t) \qquad (1)$$

where,

θ = temperature (°C),

x = space variable (cm),

t = time variable (sec),

C = volumetric heat capacity (cal/cm^3 - °C),

k = thermal conductivity (cal/sec-cm - °C), and

S = heat source term per unit volume (cal/cm^3 - sec).

Solutions of Eq. (1) were obtained for multiple-region slab models using regionwise temperature-dependent values for the thermal conductivity and volumetric heat capacity, and a time-dependent fission heat source derived from the experimental transient reactor power. The prompt fission heat source was distributed in the meat, cladding, and water regions in accordance with the breakdown given in Table III.

TABLE III

PROMPT FISSION HEAT SOURCE DISTRIBUTION IN THE CORE
(PERCENT OF 177 MeV PROMPT ENERGY RELEASE PER FISSION)

	Meat	Cladding	Water	Total
Fission Fragments	94.3	0	0	94.3
Neutrons	0	0	2.3	2.3
Prompt Gamma	0.6	1.1	1.7	3.4

Several short-period transient temperature distribution calculations were made for check-out purposes, using a three-region model consisting of regions of meat, cladding, and water, with a zero-gradient boundary condition applied at the center of the fuel plate and at the center of the coolant channel. These were nonboiling calculations; heat transfer to the water was assumed to take place by

heat conduction alone, with no account taken of convection effects in these short-period excursions. The calculations were not carried out for surface temperatures beyond saturation for lack of a sufficiently adequate understanding of boiling heat transfer.

Most of the temperature distribution calculations made involved a two-region model consisting of the meat and cladding regions of the fuel plate, with the boundary condition at the cladding surface specified by the available experimental temperature data. The meat and cladding regions were divided into a total of 10 subregions, each subregion characterized by temperature-dependent values of the volumetric heat capacity, C, and conductivity, k. These parameters were computed for each time step of the calculation by solving equations of the form $A + B\theta + C\theta^2 + D\theta^3$, where the coefficients (Table IV) were determined on the basis of a least-squares fit of the available experimental data (see Appendix A). To take account in the calculational program of the heat of fusion as each of the 10 subregions in the fuel plate reached the melting point, the subregion volumetric heat capactiy value was changed to an arbitrarily large value for a time sufficient to account for the loss of heat in fusion (see Appendix A). The arbitrary heat capacity value used was such that the temperature of the subregion rose by only 10 to 25°C during the time required to take account of the heat of fusion. Following the melting of a subregion, appropriate heat capacity and conductivity values were used for the molten material.

TABLE IV

LEAST-SQUARES-FITTED CONDUCTIVITY AND HEAT CAPACITY DATA

$\left(\left\{\begin{matrix} k \\ c \end{matrix}\right\} = A + B\theta + C\theta^2 + D\theta^3\right)$

		A	B x 10^4	C x 10^7	D x 10^{10}	Temperature Range (°C)
k Conductivity (cal/cm-sec-°C)	Meat	0.415	-1.0	0	0	20-640
		0.135	0	0	0	>640
	Cladding	0.390	2.22	-3.76	2.42	20-649
		0.170	0	0	0	>649
	Water	0.00132	0.0646	-0.414	0.827	20-150
C Volumetric Heat Capacity (cal/cm^3-°C)	Meat	0.534	3.38	-1.40	0	20-640
		0.607	0	0	0	>640
	Cladding	0.575	2.74	0	0	20-649
		0.623	0	0	0	>649
	Water	1.006	-3.45	-13.4	56.8	20-150

2. CALCULATIONAL RESULTS

Calculations were made for the 9.6-, 9.5-, 5.0-, 4.6-, and 3.2-msec-period tests for various fuel plate locations throughout the core using heat source normalization factors on the basis of the measured neutron flux distribution in the core.

Three-region calculational results for the cladding surface temperature at the flux peak position E5(7W)0 in the core are compared with the experimental data in Fig. 13. These calculations were carried out for cladding surface temperatures up to saturation, with good agreement obtained between calculation and experiment as indicated by the results shown in Fig. 13.

Two-region calculations, in which the cladding surface boundary condition was specified by the available temperature data or by reasonable extrapolations of these data, were made for three power excursion tests: (a) the 9.5-msec-period test in which no fuel plate melting occurred; (b) the 4.6-msec-period test in which some fuel plate melting occurred; and (c) the 3.2-msec-period destructive test.

2.1 The 9.5-msec-Period Test

Figs. 14 and 15 show the results of calculations made for the 9.5-msec-period test using the surface temperature data obtained at position E5(7W)0, approximately 3 in. below the core hot spot. In Fig. 14, the calculated fuel plate transient temperature distributions are shown for various times during the

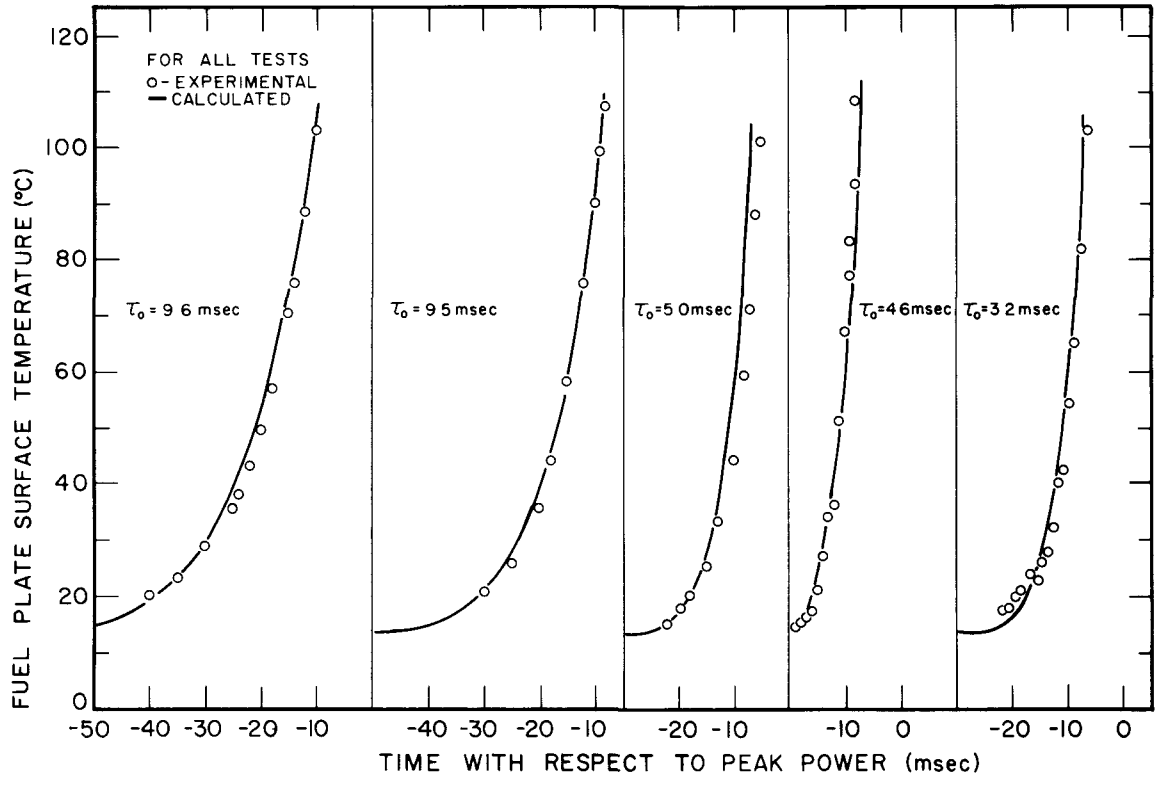

Fig. 13 Calculated and experimental fuel plate surface temperatures up to time of boiling at E5(7W)0.

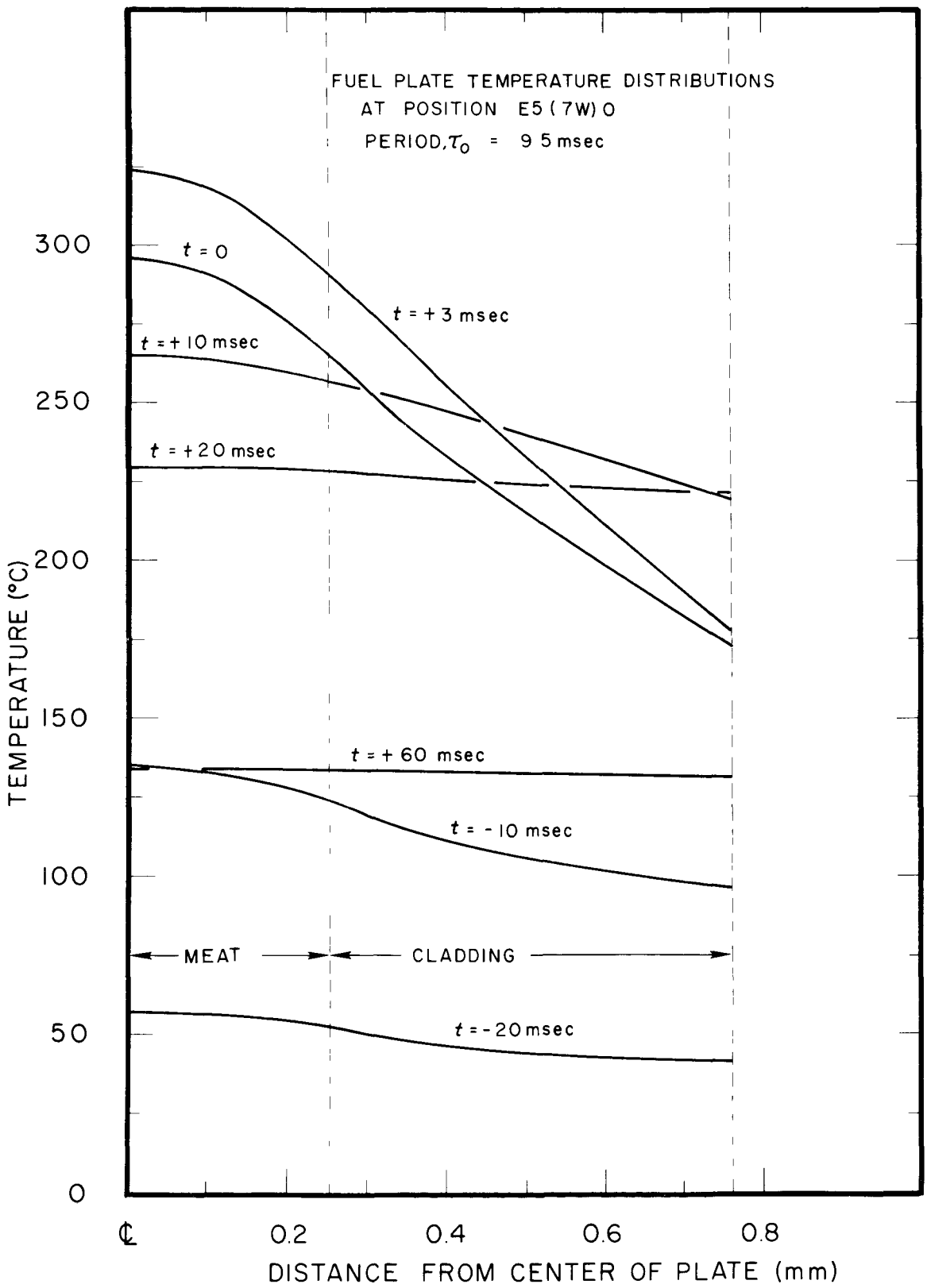

Fig. 14 Calculated fuel plate temperature distributions at E5(7W)0 for the 9.5-msec-period test.

excursion, where t = 0 specifies the time of peak power. In Fig. 15, the reactor power, fuel plate surface and central temperatures, and heat transfer rate at the plate surface are shown as functions of time during the excursion. The calculated maximum central temperature of about 320°C occurred about 3 msec after the time of peak power, at which time the surface temperature was 175°C. At a time 60 msec later, the temperature across the plate was roughly constant at about 130°C. The maximum calculated heat transfer rate of 900 cal/cm^2-sec (1.2 x 10^7 Btu/hr-ft^2) occurred 3 msec after peak power.

It is noted that the central temperature decayed rapidly with the decrease in reactor power, even though the plate surface temperature was sustained at about 200°C for a considerable length of time during the decay of the central meat temperature. The sustained high fuel plate surface temperature and low heat transfer rate to the water are indicative of an extensive film blanket covering the plate during this time.

2.2 The 4.6-msec-Period Test

For this test, the calculated fuel plate temperature distributions at position E5(7W)-3 appear in Fig. 16. In these calculations, surface temperature data from the E5(7W)-3 location (about 2 in. below the core hot spot) were used, because of early failure of the thermocouple at E5(7W)0. The onset of melting in the central portion of the fuel plate is indicated in Fig. 17 by the break in the temperature curve occurring a few msec after peak power. The plateau in the temperature curve occurring about 17 msec after the time of peak power corresponds to the restitution of the heat of fusion as the metal freezes. At the time of peak power, the calculated heat transfer rate was roughly 1600 cal/cm^2-sec (2.1 x 10^7 Btu/hr-ft^2). The maximum heat transfer rate of 2400 cal/cm^2-sec (3.2 x 10^7 Btu/hr-ft^2) occurred about 19 msec after peak power. As shown in Fig. 16, the central meat temperature reached a maximum value of about 720°C about 8 msec after peak power, at which time the surface temperature was about 530°C.

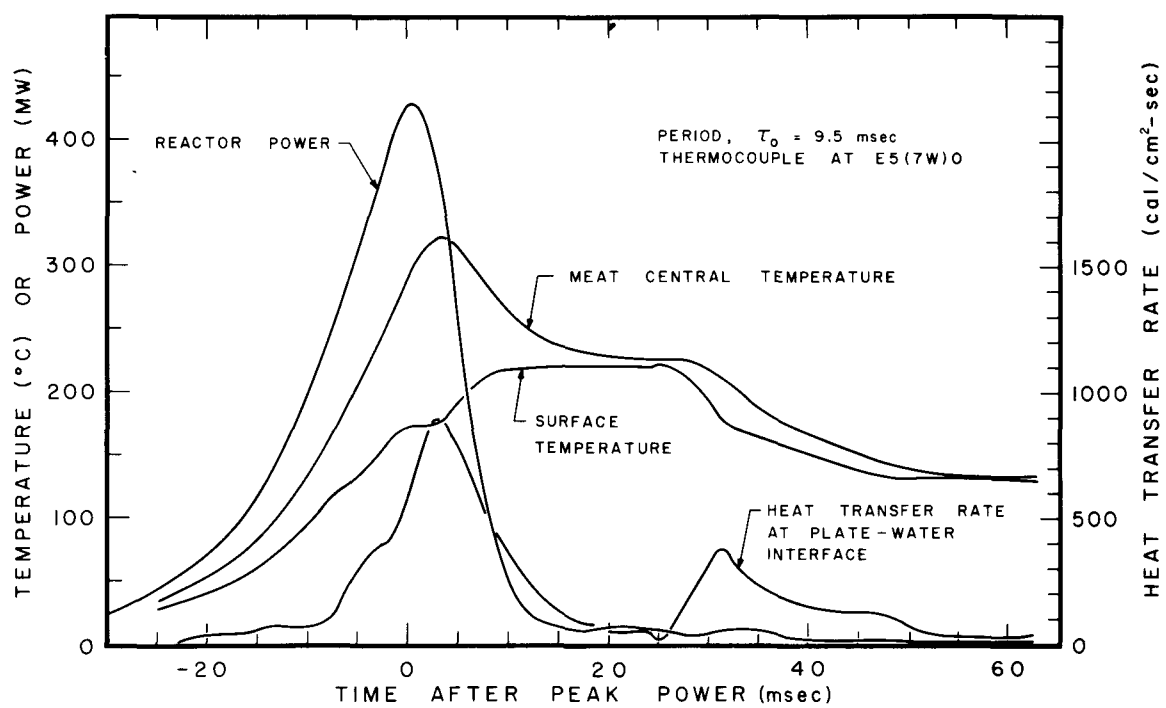

Fig. 15 Transient temperature data at E5(7W)0 for the 9.5-msec-period test.

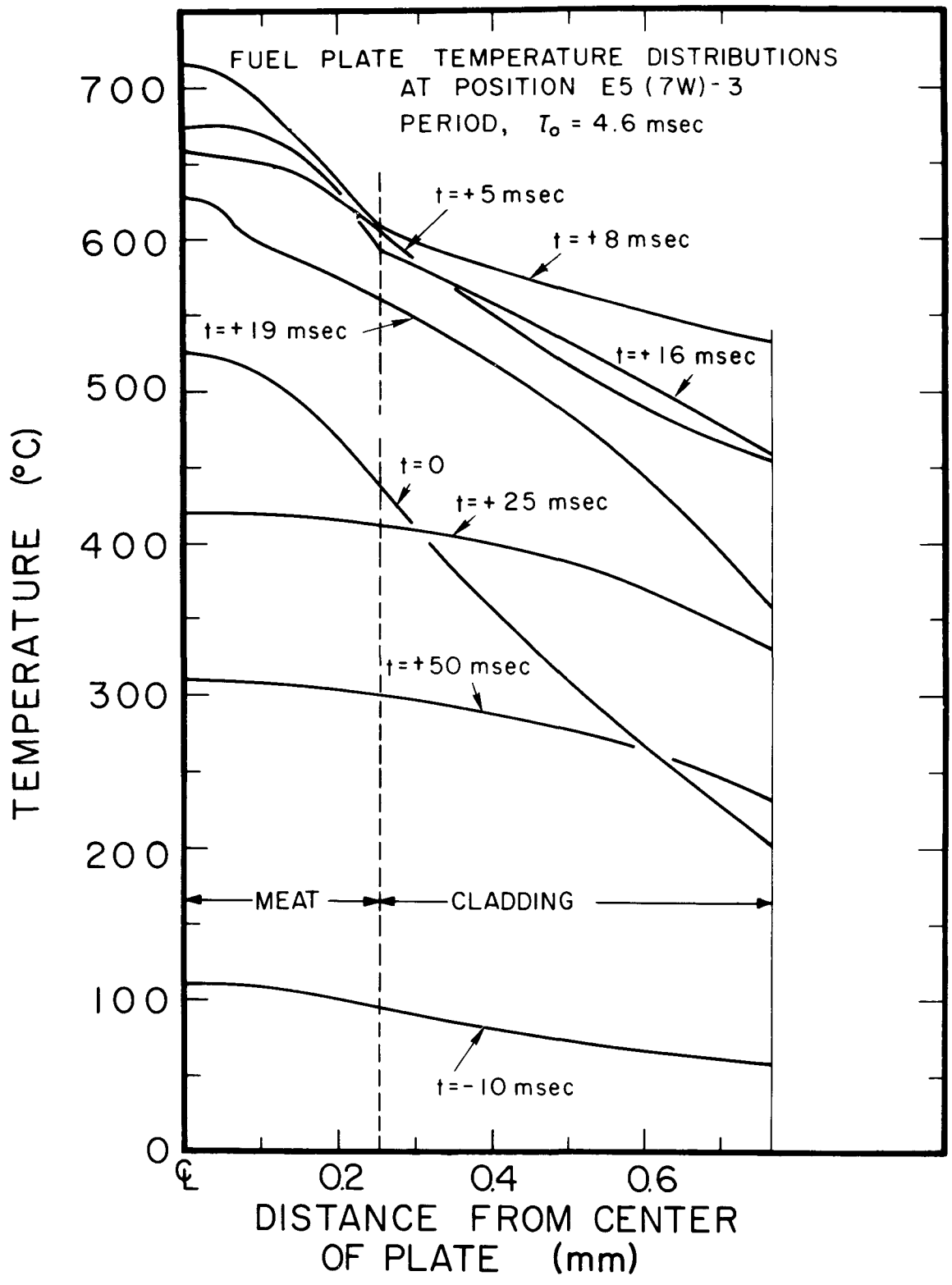

Fig. 16 Calculated fuel plate temperature distributions at E5(7W)-3 for the 4.6-msec-period test.

The correlation between the heat transfer rate and the cladding surface temperature is indicated in the curves shown in Figs. 15 and 17. In Fig. 17, for instance, the decrease in surface temperature about 17 msec after peak power corresponds to a very sharp increase in the heat transfer rate. Small variations in the experimental surface temperature trace (perhaps produced by instabilities in film boiling at the thermocouple junction) are reflected in the pronounced variations in the heat transfer rate.

2.3 The 3.2-msec-Period Test

For the destructive test case, fuel plate temperature distribution calculations were made for three fuel plate locations in the core: (a) at the core hot spot where extensive fuel plate melting occurred; (b) near the top of the core where partial fuel plate melting occurred; and (c) near the periphery of the core where no fuel plate melting occurred.

2.31 Fuel Plate Temperature Calculations (Core Hot Spot). In Fig. 18 are shown the experimental reactor power data and fuel plate surface temperature data at E5(7W)0, and the calculated fuel plate central meat temperature and heat transfer rate at the plate surface. The onset of melting in the central region is indicated by the first abrupt break in the fuel plate central temperature rise at $t \approx -1.5$ msec. A second break in the temperature rise at $t \approx 0.5$ msec is indicative of the second subregion (adjacent to the central meat subregion) undergoing melting. The fuel in the center of the plate appears to have begun to melt about one-half reactor period before peak power, at a time when the fuel plate surface temperature was only 215°C.

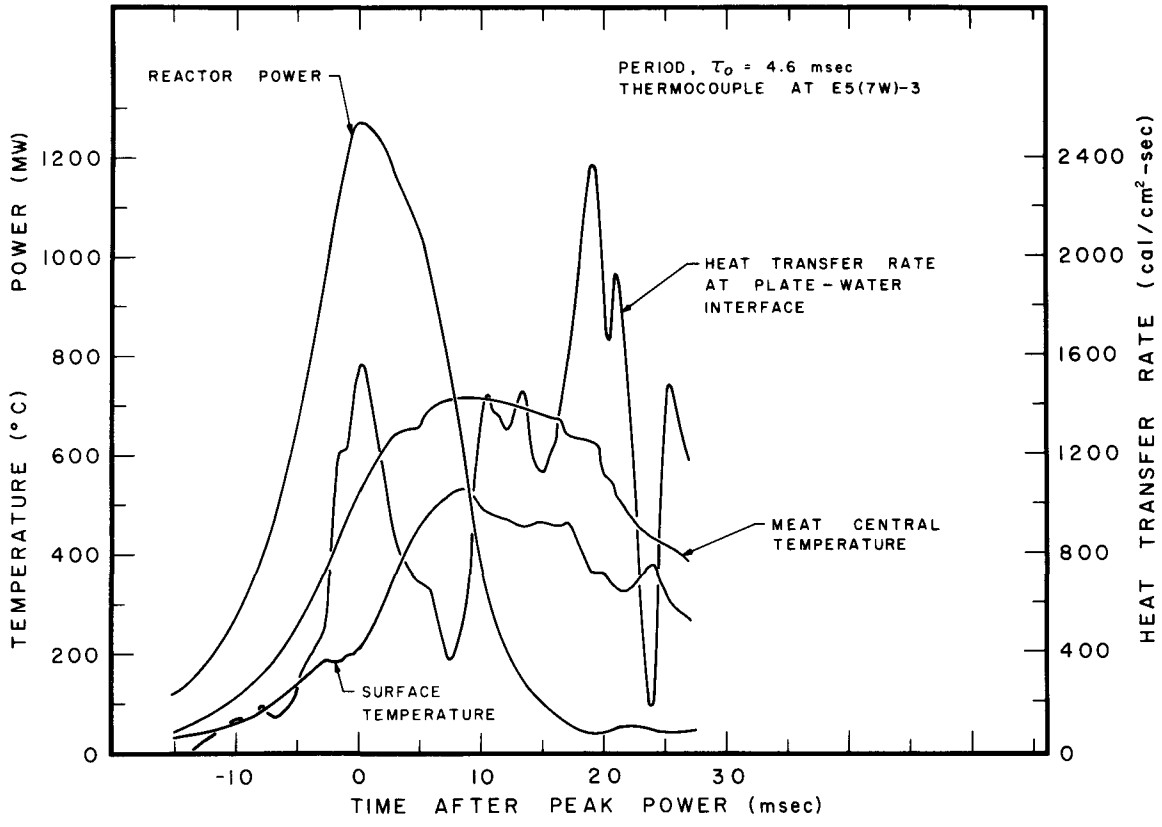

Fig. 17 Transient temperature data at E5(7W)-3 for the 4.6-msec-period test.

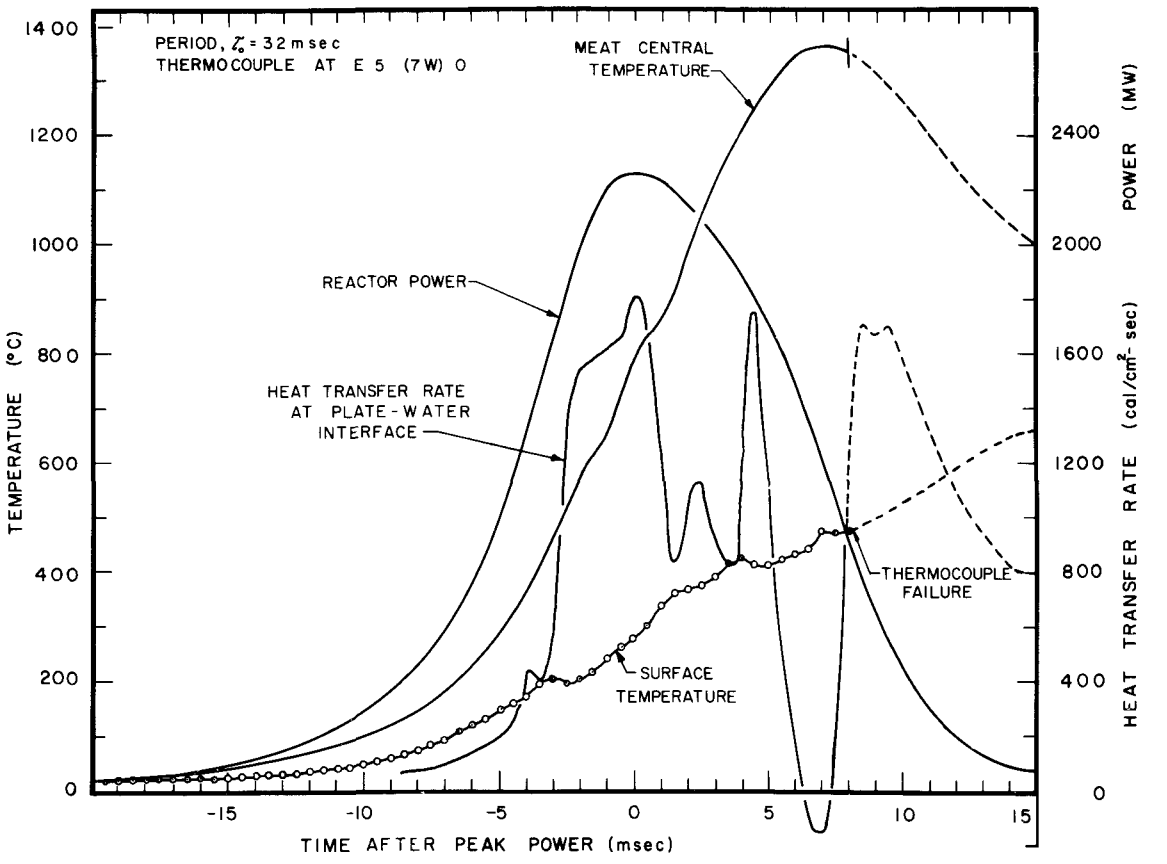

Fig. 18 Transient fuel plate temperature data at E5(7W)0 for the 3.2-msec-period test.

As shown in Fig. 18, the fuel plate surface thermocouple E5(7W)0 failed about 8 msec after the time of peak power and about 7 msec before the destructive pressure pulse. To carry out the temperature calculations during this 7 msec interval, a reasonable extrapolation of the fuel plate surface temperature was required. As shown in Fig. 19, three extrapolations were considered: (a) one in which the fuel plate surface temperature rose sufficiently to reach 665°C (in the vicinity of the aluminum melting point) at the time of the destructive pressure pulse (Trial A in Fig. 19); (b) one in which the temperature rose adiabatically (as a result, perhaps, of complete steam blanketing) from the time of thermocouple failure, reaching a temperature of about 960°C at the time of the pressure pulse (Trial C, Fig. 19); and (c) an intermediate case between Trial A and Trial C, in which the surface temperature rose linearly to a temperature of 865°C at the time of the pressure pulse.

While these postulated extrapolations assume relatively wide variations in surface temperature, they result in relatively small changes in the central meat temperature. Although larger differences in temperature are computed at the meat-cladding interface than at the fuel plate center, it is apparent (Fig. 19) that the fuel plate temperature distributions obtained with extrapolations A and B do not differ greatly except in the vicinity of the fuel plate surface. Curve A was assumed to represent a reasonably lower limit to the actual plate surface temperature rise; calculational results based on this curve are presented in Figs. 18 and 20.

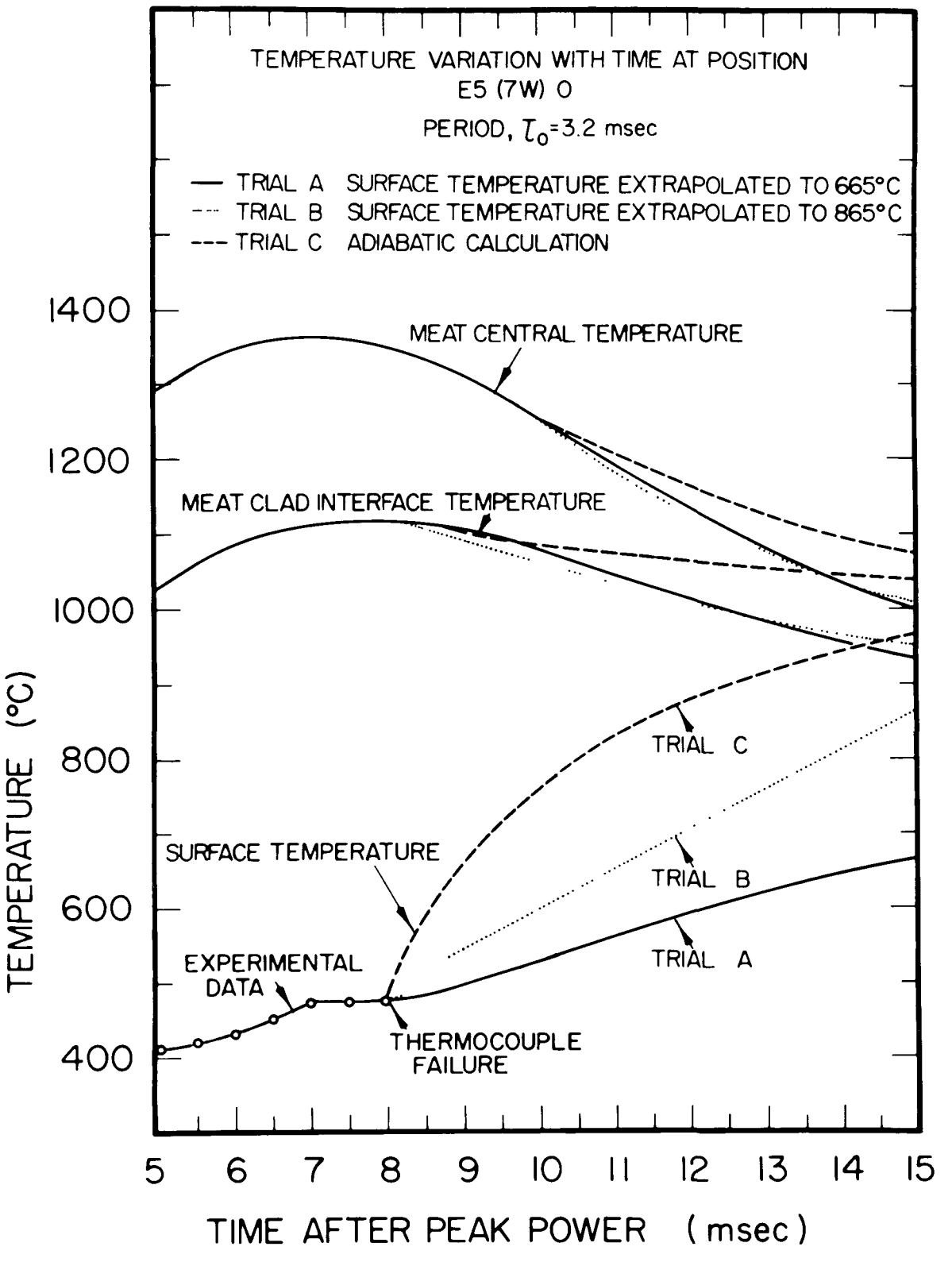

Fig. 19 Transient fuel plate temperatures at E5(7W)0 for the 3.2-msec-period test.

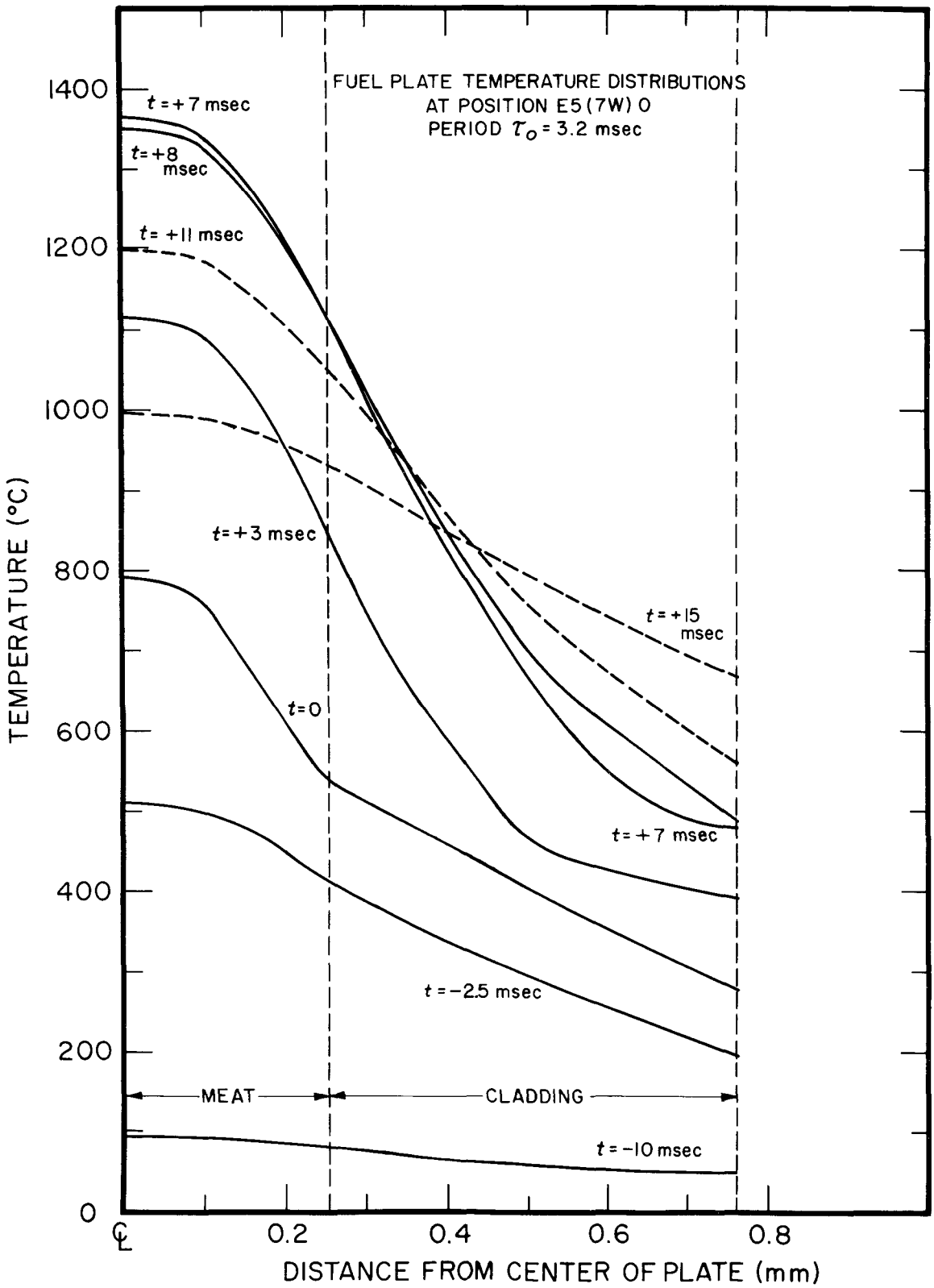

Fig. 20 Calculated fuel plate temperature distributions at E5(7W)0 for the 3.2-msec test.

Fig. 20 shows the calculated temperature distributions across the fuel plate half-thickness at various times during the excursion. The calculated central meat temperature is seen to have reached 1350°C at the time of thermocouple failure, approximately 1 msec after the peak meat temperature was obtained. At the time of core destruction, the central meat temperature had decreased to about 1000°C, while the average temperature in the plate was about 850°C.

The calculated fuel plate heat transfer rate at the core hot spot during the excursion is shown in Fig. 18. It is noted that the heat transfer rate reached a maximum value of 1800 cal/cm^2-sec (2.4 x 10^7 Btu/hr-ft^2) at about the time of peak power, in comparison with the corresponding values of 1600 and 900 cal/cm^2-sec obtained at the time of peak in the 4.6-msec test (Fig. 17) and the 9.5-msec test (Fig. 15).

2.32 Fuel Plate Temperature Calculations (Near Top of Core). Figs. 21 and 22 show the calculated fuel plate temperature behavior at position E5(12W)+6, about 6 in. above the core hot spot, during the destructive test. As shown in these figures, melting was sustained in the central region of the plate from about 2 to 11 msec after peak power. During that time, however, the temperature in the central region did not increase much above the melting point, and the calculated maximum central temperature of about 680°C was reached at a time about 6.5 msec after peak power. A maximum heat transfer rate of about 2600 cal/cm^2-sec (3.4 x 10^7 Btu/hr-ft^2) is calculated to have occurred 3.5 msec after the time of peak power. This was the largest heat transfer rate obtained in all of the calculations, exceeding the maximum rate at the core hot spot (during the same test) by nearly 50 percent.

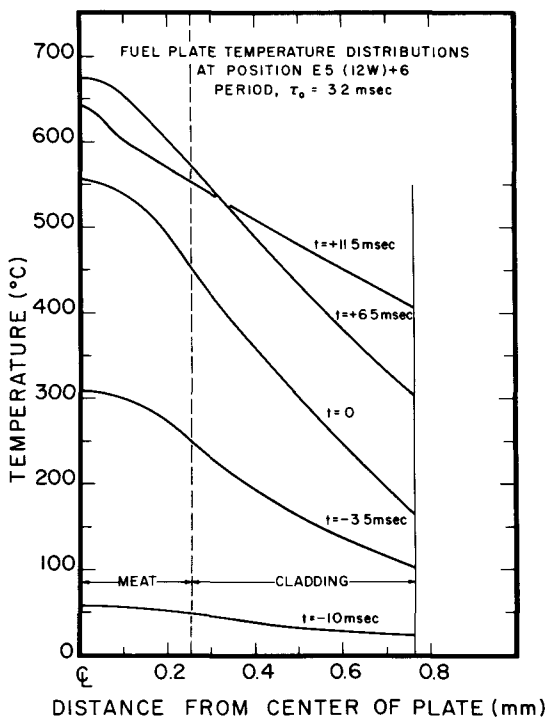

Fig. 21 Calculated fuel plate temperature distributions at E5(12W)+6 for the 3.2-msec-period test.

2.33 Fuel Plate Temperature Calculations (Near Periphery of Core). A third set of temperature calculations for the destructive test was carried out using the experimental surface temperature data obtained at the position C7(9E)0, which lies in the core centerplane, near the periphery of the core. The fuel plate temperature distributions, shown in Fig. 23, indicate that at the time of core destruction the temperature distribution through the plate was approximately uniform at about 390°C. The maximum fuel meat temperature of 430°C was reached about 5 msec after peak power. The calculated heat transfer rate (Fig. 24) reached a maximum of 1580 cal/cm^2-sec (2.1 x 10^7 Btu/hr-ft^2) about 2 msec after peak power.

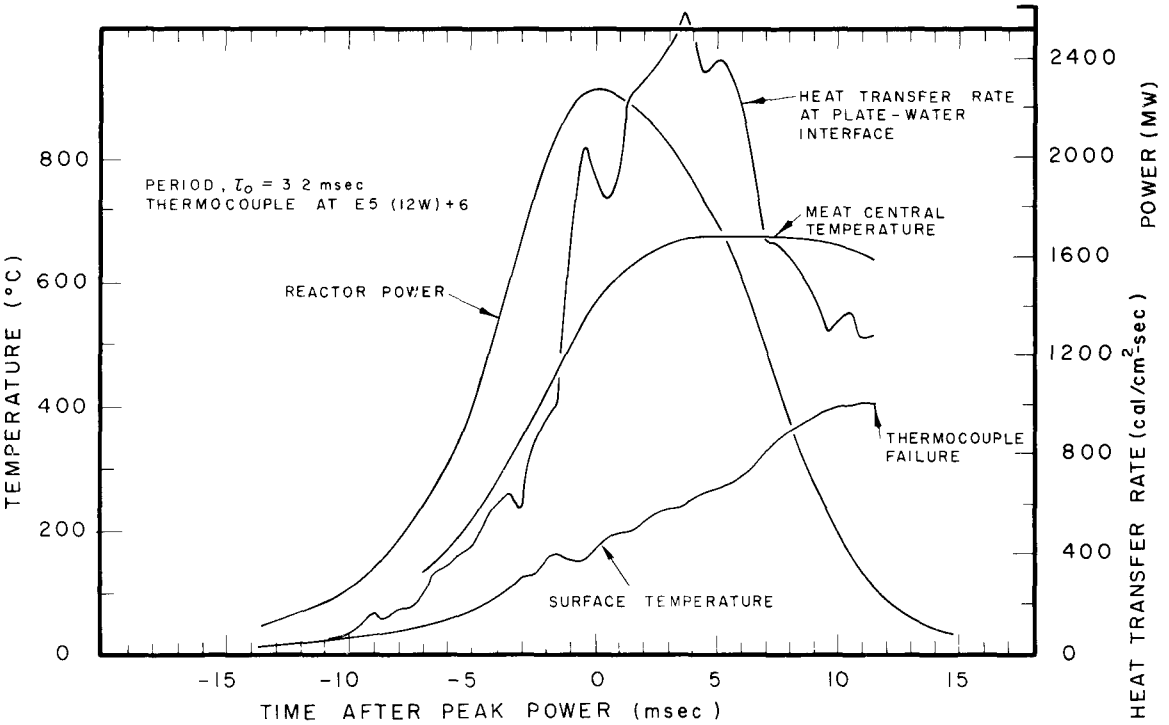

Fig. 22 Transient temperature data at E5(12W)+6 for the 3.2-msec test.

2.4 Fuel Plate Energy Partition

The fraction of the total prompt energy released to a given time that is still retained in the fuel plate at that time was calculated for each of the five transient tests studied. The results indicate that at time of peak power in each of the tests an average of about 70 percent of the fission energy released was still in the fuel plates. In the case of the 3.2-msec test, about 55 percent of the fission energy was still retained in the fuel plate at location C7(9E)0 at the time of the destructive pressure pulse.

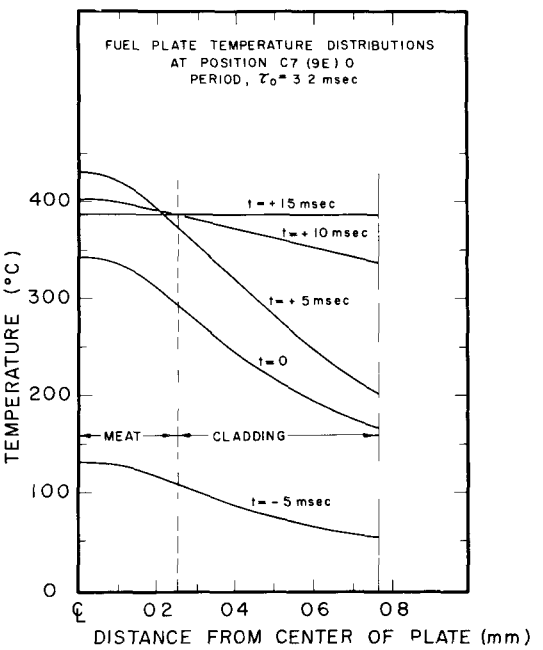

Fig. 23 Calculated fuel plate temperature distributions at C7(9E)0 for the 3.2-msec-period test.

2.5 Fuel Plate Tensile Strength and Extent of Fuel Plate Melting in the Core

Corresponding to the fuel plate temperature distributions shown in Figs. 20 and 23 are the distributions of the temperature-dependent aluminum rupture strength in Figs. 25 and 26, respectively. In both Figs. 25 and 26, the top curve ($t = -\infty$) represents the ambient-temperature, ultimate tensile strength ($\approx$45,000 psi [8]) at each point in the meat and cladding at the start of the excursion.

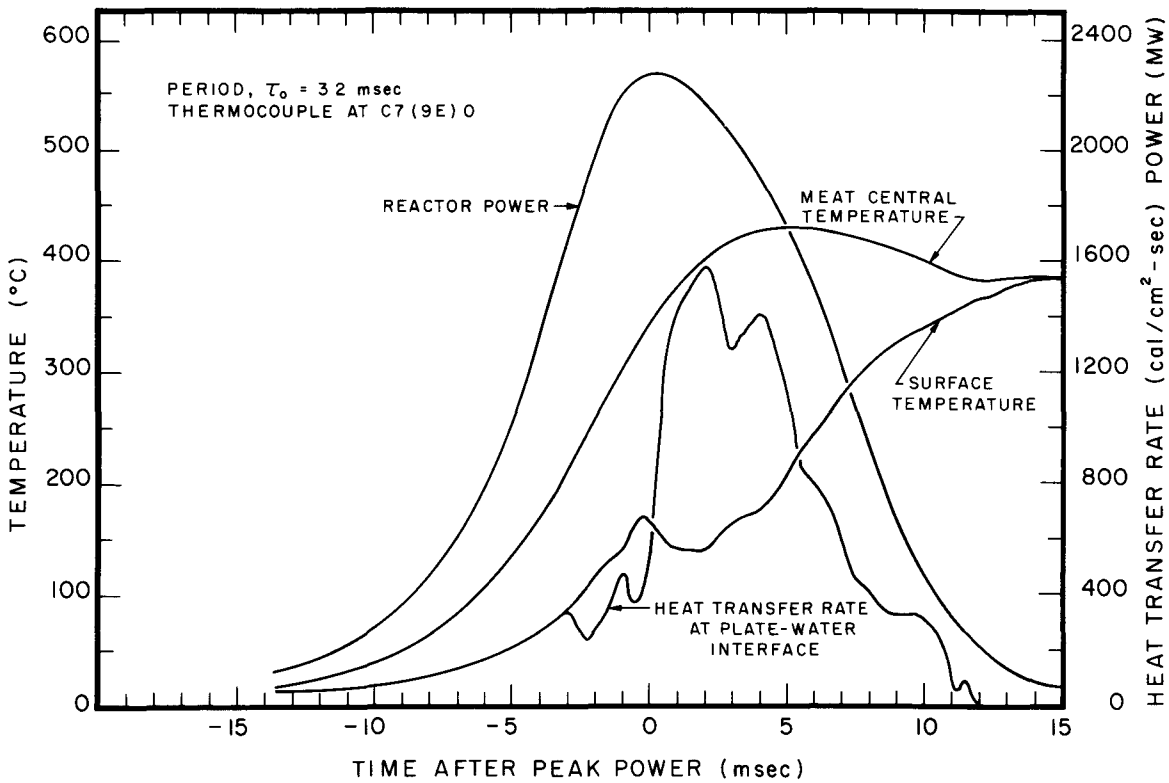

Fig. 24 Transient temperature data at C7(9E)0 during the 3.2-msec-period test.

At the core hot-spot position of E5(7W)0, the rupture strength of the meat alloy was essentially negligible at the time of peak power, while the cladding strength was roughly a factor of 10 lower than its initial strength (Fig. 25). At a time approximately 8 msec after peak power, the tensile strength of the entire fuel plate in the center of the core was essentially gone.

At the core peripheral position of C7(9E)0, the rupture strength of the meat alloy at the time of peak power had decreased to about 10 percent of its initial value, while the cladding strength had been reduced to roughly 30 percent of its initial value (Fig. 26). At the time of the destructive pressure pulse (t = 15 msec), the average fuel plate tensile strength near the periphery of the core was only about 6 percent of its initial strength.

Calculations for the fuel plate temperature and tensile strength at other points in the core at the time of the destructive pressure pulse also were made on the basis of the cladding surface thermocouple data available. At other points where surface temperature experimental data were not available, estimates of the fuel temperature and tensile strength at the time of core destruction were obtained on the basis of the power distribution across the core (as deduced from the experimental static flux distribution data, corrected for the effect of the change in control rod position) and the transient fuel plate energy partition behavior (obtained by interpolation and extrapolation of the calculated behavior for fuel plate positions where thermocouple data were available). The results of such calculations for various points throughout the core indicate that at the time of the destructive pressure pulse the fraction of fuel plates in the core which

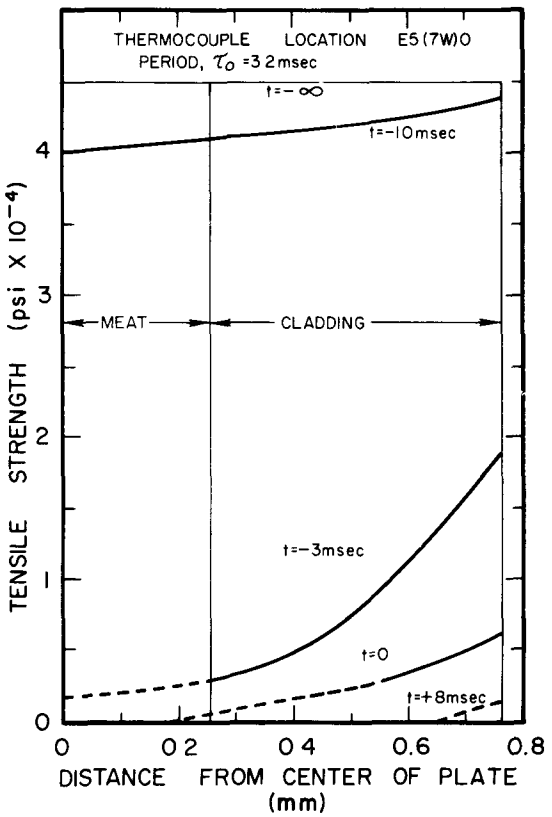

Fig. 25 Tensile strength in the fuel plate at E5(7W)0 during the 3.2-msec-period test.

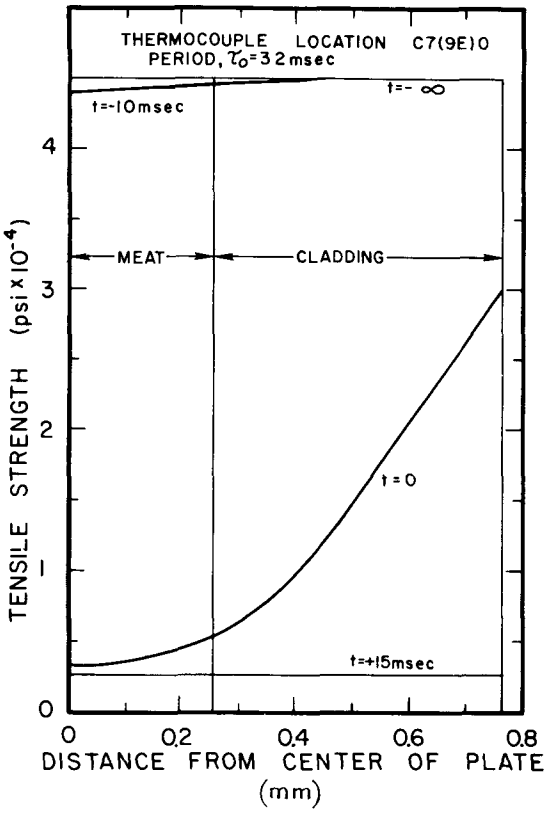

Fig. 26 Tensile strength in the fuel plate at C7(9E)0 during the 3.2-msec-period test.

were molten across the entire fuel plate thickness was 8 percent, but that approximately one-third of the entire fuel plate volume in the core had reached the melting point of aluminum. Since the tensile strength of type-6061 aluminum at 375°C is only about 7 percent of the ambient temperature value, and effectively negligible near the melting point [8], it is reasonable to expect that at the time of the destructive pressure burst a large portion of the quasi-molten plates were in a physical state which would permit a large scale fragmentation and dispersal of the fuel plates by one or more mechanisms, such as a pressure wave propagated throughout the core, mechanical vibration of the core structural components, etc. The calculated volume of molten fuel plate material is not inconsistent with the fact that 35 percent of the fuel plate volume in the core was not recovered intact after the final 3.2-msec destructive burst [4].

V. DISCUSSION OF RESULTS

Several important features of the fuel plate temperature behavior in the destructive test may be examined with respect to the problem of nuclear safety of water-moderated, plate-type reactors. In particular, consideration may be given to those aspects which bear on the problems of (a) the importance of the metal-water chemical reaction in a violent accident, and (b) the question of the systematics of nuclear excursion behavior in a destructive accident.

In the hazards evaluation of heterogeneous water-moderated reactors, consideration is given to the possibility of achieving sufficiently high temperatures to cause melting or vaporization of the metallic fuel elements, which could then exothermically react with the water to give an explosive chemical energy release. The analysis of the debris in the vessel [2,4], following the destructive 3.2-msec-period test, indicated that about 0.4 percent of the aluminum in the D Core actually burned, yielding about 3.5 MW-sec of chemical energy.

Had this aluminum burned as rapidly as an explosive, this amount of energy could have produced the severe damage which was obtained in the D Core. However, there is evidence indicating that the extent and rate of the aluminum-water reaction are low unless extremely high temperatures (above 1700 to 1800°C) are achieved [9]. On the basis of these results, the 1300 to 1400°C maximum fuel plate temperatures that were achieved during the Spert I destructive test imply that the aluminum-water reaction proceeded slowly relative to the time scale of the destructive pressure burst. Hence, as a mechanism for providing the high heat transfer rates required to explain the very rapid destructive pressure burst, the metal-water reaction appears to be a poor candidate. The mechanism of rapid plate fragmentation, on the other hand, would give the necessary heat transfer rates, and might also be instrumental in enhancing whatever chemical reaction there was by permitting the hot interior portions of the fuel plates to be directly exposed to the water.

A rough comparison may be made of the Spert I chemical energy release with the estimated chemical energy generated in the SL-1 accident. The Spert I chemical energy release was about 10 percent of the nuclear release, whereas in the SL-1 accident, the fraction was about 18 percent. While a quantitative comparison is not feasible, the more extensive chemical reaction of the SL-1 excursion can probably be associated with the higher fuel temperatures obtained in SL-1, which have been estimated [10] to have reached higher than the region of the aluminum vaporization point of 2040°C, well above the 1300-1400°C maximum fuel temperature reached in Spert I. Thus, on the basis of the aluminum-water reaction rate data, the SL-1 chemical reaction would appear to have occurred in the temperature domain where the rate and extent of oxidation of aluminum increase rapidly with temperature, whereas the Spert I reaction was in the domain where the rate and extent of burning are low. It might be expected that if a shorter period, more severe Spert destructive excursion had been run (with more fission energy release and higher fuel temperatures), a more vigorous and relatively greater chemical contribution to the total energy output would have been achieved than that which was obtained in the actual 3.2-msec-period test.

Of major significance in the destructive test was the observation that, prior to the onset of the destructive pressure burst, the reactor underwent a self-limiting power excursion, with burst characteristics predictable from the longer-

period test data. The post nuclear burst occurrence of the destructive pressure pulse can be interpreted in terms of (a) the time required to attain in a significant number of fuel plates a loss of tensile strength (effectively, a molten state) sufficient to permit rapid plate fragmentation; (b) the time required to develop a mechanism for initiating the postulated rapid fragmentation of the hot fuel plate material; and (c) the time required to propagate throughout the core the effects of fuel dispersal, heat transfer, and subsequent steam pressure buildup.

Although the central part of the fuel plates in the core hot spot were already melting before the time of peak power (Fig. 18), roughly 10 msec were required for the melting process to progress to the surface of the cladding. As indicated in Figs. 20, 21, 23, 25, and 26, the loss of tensile strength elsewhere in the core also proceeded rapidly during this interval of time. Thus, the attainment of a weakened fuel plate condition that could permit an easy breakup of a sizeable number of fuel plates was not obtained until after the nuclear excursion had been effectively terminated.

With respect to the initiation of fuel plate fragmentation and dispersal at one or more points in the core, a number of trigger mechanisms can be postulated, one of these involving the effects of a steam explosion arising from the entrapment and superheating of small quantities of water in a molten metal environment. Such a mechanism does not appear unreasonable in view of the pattern of fuel-plate thermal deformation obtained in the longer period tests of the D Core, where extensive channel blockage and fusion of melted fuel plates were found to have occurred [1, 4].

VI. REFERENCES

1. A. H. Spano and R. W. Miller, Spert I Destructive Test Program Safety Analysis Report, IDO-16790 (June 1962).

2. R. W. Miller et al, Report on the Spert I Destructive Test Program on an Aluminum, Plate-Type, Water-Moderated Reactor, IDO-16884 (May 1964).

3. M. R. Ziessler, Non-Destructive and Destructive Transient Tests of the Spert I-D, Fully-Enriched, Aluminum-Plate-Type Core: Data Summary Report, IDO-16886 (November 1963).

4. J. Dugone and D. D. Wieland, Fuel Plate Experience During the Spert I Destructive Test Series with an Aluminum-Clad, Plate-Type Core, IDO-16885 (July 1963).

5. Quarterly Technical Report Spert Project, Fourth Quarter 1959, IDO-16616 (August 1960) pp 21-24.

6. H. Emmons, "Theory and Application of Extended Surface Thermocouples", J. Franklin Inst. 229 n 1 (January 1940) pp 29-52.

7. R. J. Wagner, HEAT-I, A One Dimensional Time Dependent or Steady State Heat Conduction Code for the IBM-650, IDO-16867 (April 1963).

8. T. Lymas (ed.), Metals Handbook. Vol. 1, Properties and Selection of Metals, 8th ed. Metals Park Novelty, Ohio: American Society for Metals, 1961, pp 945, 996, 1196, 1226.

9. R. O. Ivins, "A Study of the Reaction of Aluminum/Uranium Alloy Fuel Plates with Water Initiated by a Destructive Reactor Transient", Trans. Am. Nucl. Soc., 6 (June 1963) pp 101-102.

10. J. F. Kunze (ed.), Final Report of SL-1 Recovery Operations May 1961 Through July 1962, IDO-19311 (July 1962).

11. S. J. Paprocki and R. F. Dickerson, "Reactor Materials Properties", Nucleonics, 18 (November 1960) p 155.

12. H. Etherington (ed.), Nuclear Engineering Handbook, New York: McGraw-Hill Book Company, Inc., 1958, pp 10-30.

13. M. Holt et al, "Aluminum and Aluminum Alloys for Pressure Vessels", Welding Research Council Bulletin, (February 1962) p 75.

14. C. R. Tipton, Jr., Reactor Handbook. Vol. 1, Materials, 2nd Revision. New York: Interscience 1960, pp 174, 484.

15. M. Hanson and K. P. Anderko, Constitution of Binary Alloys, 2nd ed. New York: McGraw-Hill Book Company, Inc., 1958, p 143.

16. E. Epremian (ed.), Uranium Alloy Newsletter No. 14, WASH-296 (March 1956) p 27, 12:7209.

17. R. Boucher, Diffusion of Aluminum During the Transformation UAl_3-UAl_4 in the Solid State, AEC-TR-4768 (July 1958).

18. W. D. Treadwell and L. Terebisi, "Energy of Formation of Aluminum Oxide from the Elements", Helv. Chim. Acta., 16 1933, p 937.

19. A. R. Kaufmann (ed.), Nuclear Reactor Fuel Elements, Metallurgy and Fabrication, New York: Interscience Publishers, 1962, p 36.

20. C. D. Harrington and A. E. Ruehle (eds.), Uranium Production Technology, Princeton: D. Van Nostrand Co., Inc., 1959, pp 296-297.

21. Aluminum Research Laboratories, England, Personal Communication (December 1962).

22. Aluminum Company of America, Alcoa Research Laboratories, letter from L. A. Willey to L. P. Smith Re: 1027-62A (July 11, 1962).

23. W. O. Schaffnit, Metallurgical Examination of a Melted Spert I Type-B Fuel Plate, IDO-16477 (September 1958) pp 15-16.

24. D. W. Rhodes, Phillips Petroleum Company, AED, Personal Communication (February 1963).

25. R. Abramson et al, "Some Properties of Plutonium and Aluminum-Plutonium Alloy," Proceedings of the Second United Nations Conference on the Peaceful Uses of Atomic Energy held in Geneva 1 September-13 September 1958, A/Conf.15/P/327, 1958.

26. Reactor Materials, A Quarterly Tech. Prog. Rev., Vol. 5 No. 4 (November 1962) p 20.

APPENDIX A

THERMAL PROPERTIES OF THE SPERT I-D CORE FUEL PLATES

APPENDIX A

THERMAL PROPERTIES OF THE SPERT I-D CORE FUEL PLATES

1. FUEL PLATE CHARACTERISTICS

The Spert I-D core fuel plate consisted of a 20-mil-thick, 93 percent-enriched uranium-aluminum alloy meat section, clad on both sides with 20-mil-thick claddings of type-6061 aluminum. Fuel plate characteristics are given in Table A-I.

TABLE A-I

SPERT I-D CORE FUEL PLATE CHARACTERISTICS

Enrichment (% U-235)	93%
Mass of U-235 per plate (nominal)	14 g
Mass of U per plate	15.1 g
Meat length (nominal)	24.4 in.
Meat width (nominal)	2.45 in.
Meat thickness (nominal)	0.020 in.

2. THERMAL PROPERTIES OF THE MEAT ALLOY

2.1 Uranium Weight Fraction

Experimentally determined densities of dilute uranium alloys at room temperature are shown in Table A-II [11].

These experimental data for dilute uranium-aluminum alloy material may be represnted by

$$y = 0.8793 - \frac{2.0644}{\rho} \qquad \text{(A-1)}$$

where y is the weight percent of uranium in the alloy and ρ is the alloy density given by

$$\rho = \frac{M}{yV} \qquad \text{(A-2)}$$

where M is the mass of uranium in the volume, V, of the alloy. From the above data, y for the Spert I meat alloy is determined to be 23.8 percent.

TABLE A-II

PROPERTIES OF DILUTE URANIUM ALLOYS

Aluminum-Uranium Alloy (wt %)	Uranium Density (g/cm3)	Alloy Density (g/cm3)
16	0.458	2.87
25	0.820	3.28
35	1.39	3.9
Unalloyed Uranium	19.04	19.04

2.2 Coefficient of Linear Expansion ($\theta < 640°C$)

The linear expansion coefficient, $\lambda\theta$, of uranium-aluminum alloys is given in Ref. 12 for alloys having uranium contents of 0, 12.5, 22.7, and 30.5 wt%. The corresponding data for 23.8 wt% alloy (obtained by interpolation of the data in Ref. 12) can be represented by

$$\lambda_\theta = 18.7 \times 10^{-6} + 1.45 \times 10^{-8}\ \theta - 1.29 \times 10^{-11}\ \theta^2 \qquad \text{(A-3)}$$

from which the linear expansion data in Table A-III were derived.

TABLE A-III

AVERAGE LINEAR EXPANSION COEFFICIENT OF 23.8 WT% U-AL ALLOY

Temperature Range (°C)	λ_θ (Eq. A-3) (10-6/°C)
20-100	20.00
20-200	21.06
20-300	21.87
20-400	22.42
20-500	22.72
20-600	22.75
20-640	22.70

Using Eq. A-3, the volumetric expansion and density of the meat were computed as a function of temperature. The variation of meat density with temperature for $\theta < 640°C$ is given in Table A-IV on page 39.

2.3 Volumetric Heat Capacity ($\theta < 640°C$)

The specific heat of 23.8 wt% U-Al alloy was estimated on the basis of the known specific heats of uranium and aluminum, and their weight fractions in the meat alloy. The values for the specific heat, c(cal/g-°C), and the volumetric heat capacity, C(cal/cm^3-°C), as a function of temperature are given in Table A-IV. The volumetric heat capacity data for the Spert I meat alloy for $\theta < 640°C$ are represented by the equation

$$C(\text{cal/cm}^3\text{-°C}) = 0.534 + 3.38 \times 10^{-4}\ \theta - 1.40 \times 10^{-7}\ \theta^2. \qquad \text{(A-4)}$$

2.4 Thermal Conductivity ($\theta < 640°C$)

Experimental thermal conductivity measurements on forged bars of 12.5, 22.7, and 30.5 wt% U-Al alloy material were made in the temperature range from 150 to 400°C [13]. Interpolation of the data obtained yielded values of the thermal conductivity for the Spert I 23.8 wt% meat alloy (Table A-IV). These values are represented by the equation

$$k(\text{cal/sec-cm-°C}) = 0.415 - 1.00 \times 10^{-4}\ \theta \qquad \text{(A-5)}$$

which is applied in the Spert I temperature calculations for the temperature range from 25 to 640°C.

2.5 Meat Density ($\theta > 640°C$)

Data on the density change of U-Al alloys for temperatures greater than 640°C have not been found in the literature. An estimate of the density variation may be made by considering the case of 1 g of a 23.8 wt% U-Al alloy of eutectic composition. The phase diagram [14, 15] yields the following data:

TABLE A-IV

THERMAL PROPERTIES OF 23.8 WT% U-Al ALLOY

($\theta < 640°C$)

Temperature (°C)	Density (g/cm^3)	Specific Heat (cal/g-°C)	Volumetric Heat Capacity (cal/cm^3-°C)	Conductivity (cal/sec-cm°C)
25	3.22	0.167	0.538	
50	3.22	0.171	0.551	
100	3.21	0.178	0.569	
150	3.20	0.183	0.585	0.400
200	3.18	0.188	0.599	0.395
250	3.17	0.193	0.612	
300	3.16	0.197	0.623	0.386
350	3.15	0.201	0.634	
400	3.14	0.205	0.645	0.375
450	3.13	0.209	0.655	
500	3.12	0.213	0.665	
550	3.11	0.217	0.675	
600	3.10	0.222	0.686	
640	3.09	0.225	0.695	

(1) $\theta < 640°C$ (a) Solid Phase: Al = 0.654 g
(b) Solid Phase: UAl_4 (U = 68.81% or 0.238 g; Al = 31.19% or 0.108 g)

(2) $\theta = 640°C$ (a) Liquid Phase: U-Al (U = 13% or 0.105 g; Al = 87% or 0.702 g)
(b) Solid Phase: UAl_4 (U = 68.81% or 0.133 g; Al = 31.19% or 0.060 g)

(3) $\theta_- = 730°C$ (a) Liquid Phase: U-Al (U = 18% or 0.160 g; Al = 82% or 0.726 g)
(b) Solid Phase: UAl_4 (U = 68.81% or 0.078 g; Al = 31.19% or 0.036 g)

(4) $\theta_+ = 730°C$ (a) Liquid Phase: U-Al (U = 18% or 0.162 g; Al = 82% or 0.736 g)
(b) Solid Phase: UAl_3 (U = 74.63% or 0.076 g; Al = 25.37% or 0.026 g)

(5) $\theta = 940°C$ [16] (a) Liquid Phase: U-Al (U = 0.238 g; Al = 0.726 g)

The volume increase when aluminum melts is 6.6 percent [14]. The volume increase during the transformation $UAl_3 + Al \rightarrow UAl_4$ is 1.6% [17]. When θ = 640°C, the aluminum solid phase (0.654 g) undergoes a volume increase in melting of 6.6 percent, and a part of the aluminum (0.048 g), which was in the form of UAl_4 (density 5.7 g/cm^3), melts, producing an additional increase in volume. A part of the uranium (0.105 g) in the form of UAl_4 becomes liquid uranium (density $\approx$ 18.4 g/cm^3). This corresponds to a decrease in volume. The UAl_4 phase weight decreases by 0.153 g, corresponding to a decrease in volume. The net total effect is computed to be an increase in total volume of about 4.3 percent. Therefore, the alloy density at 640°C following the phase change is equal to

$$\rho = \frac{3.087}{1.043} = 2.96 \text{ g/cm}^3. \qquad \text{(A-6)}$$

When the temperature increases from 640 to 730°C, two expansion effects have to be considered: (a) the volumetric change resulting from the change in phase, and (b) the volumetric increase due to heating.

(a) A part of the uranium (0.55 g) in the form of UAl_4 melts, resulting in a decrease in volume. A part of the aluminum (0.024 g) in the form of UAl_4 melts, resulting in an increase in volume. The UAl_4 phase weight decreases by 0.079 g, corresponding to a decrease in volume. The net total effect appears to be negligible since it results from the transformation of small masses.

(b) Most of the alloy is in the form of liquid aluminum. Assuming that the linear expansion coefficient of aluminum is about 29 x 10^{-6}/°C in the temperature range 640 to 730°C, the corresponding volume increase will be equal to 3 x 29 x 10^{-6} x 90 = 0.8 percent. Thus, the density of the alloy at 730°C is equal to ρ = 2.96/1.008 = 2.94 g/cm^3.

When the temperature reaches 730°C, a peritectic transformation is obtained in which UAl_4 is changed to UAl_3, with an associated volume decrease of 1.6 percent. However, since the transformation affects only a small portion of the alloy (0.114 g), the resulting volume change may be neglected.

In summary: (a) when the temperature reaches 640°C, the density of the alloy changes from 3.09 to 2.96 g/cm^3, and (b) between 640 and 730°C, the density of the alloy decreases by about 0.8 percent to a value of 2.94 g/cm^3.

2.6 Specific Heat ($\theta > 640$°C)

Following Treadwell and Terebese [18], the following slowly-varying temperature dependence has been assumed for the specific heat of molten aluminum in the temperature range from 640 to 2300°C:

$$c(\text{cal/g-°C}) = 0.255\ [1 + 1.87 \times 10^{-4}\ (\theta - 640)]. \qquad \text{(A-7)}$$

Assuming the same temperature dependence to hold for uranium, and using 0.046 cal/g-°C for the specific heat of uranium at 640°C [19, 20], the specific heat of 23.8 wt% U-Al alloy will change with temperature in the range $640 < \theta <$ 2300°C in accordance with

$$c(\text{cal/g-°C}) = 0.0205\ [1 + 1.87 \times 10^{-4}\ (\theta - 640)]. \qquad \text{(A-8)}$$

This slow increase in the specific heat of the alloy as the temperature rises, combined with the corresponding slow decrease in density, results in an essentially constant value of the volumetric heat capacity of the alloy for temperatures above the melting point. This value has been taken to be

$$C = (2.96\ g/cm^3)(0.205\ cal/g\text{-}°C) = 0.61\ cal/cm^3\text{-}°C. \qquad (A\text{-}9)$$

2.7 Thermal Conductivity ($\theta > 640°C$)

From Eq. A-5 the conductivity of the meat alloy at 640°C is equal to 0.351 cal/sec-cm°C. A literature search has not yielded information on the conductivity of molten U-Al alloys. For pure aluminum, the conductivity at the melting point is 0.537 cal/sec-cm-°C; for molten aluminum up to 800°C, the conductivity remains approximately constant at 0.207 cal/sec-cm-°C [21]. Assuming a corresponding change in the conductivity of the meat alloy for $\theta >$ 640°C, the following is obtained:

$$k = 0.351 \times \frac{0.207}{0.537} = 0.14\ cal/sec\text{-}cm\text{-}°C \qquad (A\text{-}10)$$

3. CLADDING

3.1 Volumetric Heat Capacity and Conductivity ($\theta < 649°C$)

Table A-V presents data on the volumetric heat capactiy [13] and conductivity [22] of type-6061 aluminum for temperatures up to 649°C.

Based on these data, the heat capacity and conductivity for $\theta < 649°C$ can be represented by the following equations:

$$C(cal/cm^3\text{-}°C) = 0.575 + 2.74 \times 10^{-4}\ \theta \qquad (A\text{-}11)$$

$$k(cal/sec\text{-}cm\text{-}°C) = 0.390 + 2.22 \times 10^{-4}\ \theta - 3.76 \times 10^{-7}\ \theta^2 + 2.42 \times 10^{-10}\ \theta^3. \qquad (A\text{-}12)$$

3.2 Volumetric Heat Capacity and Conductivity ($\theta > 649°C$)

The cladding material of aluminum 6061 contains approximately 0.6 percent silicon by weight. There is a "hot-shortness" temperature range from 662 to 649°C [8, 23], ie, at 622°C melting begins at the grain boundaries, with the entire alloy molten at 649°C. Assuming (a) the volume increase when Al-6061 melts to be the same as that for pure aluminum (ie, 6.6 percent) and (b) the change in heat capacity of Al-6061 to be the same as that for pure aluminum (ie, 13.3 percent), the following is obtained:

$$C(cal/cm^3\text{-}°C) = \frac{0.753}{1.066 \times 1.133} = 0.62 \qquad (A\text{-}13)$$

assumed constant for $\theta > 649°C$.

TABLE A-V

VOLUMETRIC HEAT CAPACITY AND THERMAL CONDUCTIVITY OF Al-6061

($\theta < 649°C$)

Temperature (°C)	Volumetric Heat Capacity (cal/cm^3-°C)	Thermal Conductivity (cal/sec-cm-°C)
0		0.39
25	0.582	
50	0.590	
100	0.603	0.41
150	0.616	
200	0.630	0.42
250	0.644	
300	0.657	0.43
350	0.671	
400	0.685	0.43
450	0.698	
500	0.712	0.44
550	0.726	
600	0.740	0.44
622	0.746	
649	0.753	

Assuming the change in thermal conductivity as Al-6061 melts to be the same as that for pure aluminum (Section 2.8, above) we obtain for $\theta > 649°C$:

$$k(\text{cal/sec-cm-°C}) = 0.441 \times \frac{0.207}{0.537} = 0.17 \qquad \text{(A-14)}$$

4. WATER

4.1 Volumetric Heat Capacity and Thermal Conductivity

Least-squares fits of the available data on volumetric heat capacity and thermal conductivity for pressurized water for $\theta \leq 150°C$ yield the following relations [24]:

$$C(\text{cal/cm}^3\text{-°C}) = 1.006 - 3.45 \times 10^{-4}\,\theta - 1.34 \times 10^{-6}\,\theta^2 + 5.68 \times 10^{-9}\,\theta^3 \qquad \text{(A-15)}$$

and

$$k(\text{cal/sec-cm-°C}) = 1.32 \times 10^{-3} + 6.46 \times 10^{-6}\,\theta - 4.14 \times 10^{-8}\,\theta^2 + 8.27 \times 10^{-11}\,\theta^3. \qquad \text{(A-16)}$$

5. HEAT OF FUSION

5.1 Heat of Fusion of Meat Alloy and Melting Approximation

Data on the phase composition of unit mass of 23.8 wt% U-Al alloy are given in Section 2.5 of Appendix A. It is shown that at 640°C, 0.153 g of the UAl_4-solid phase and 0.654 g of the aluminum-solid phase melt, resulting in the total melting of 0.807 g of the alloy. From 640 to 730°C, an additional 0.079 g of the UAl_4 melts. At 730°C, 0.012 g of UAl_4 melts as a result of the peritectic transformation at that temperature, and, finally, 0.102 g of UAl_3 melts between 730 and 940°C.

The heat of fusion of the eutectic mass present in various uranium-aluminum alloys has been determined experimentally [25]. Interpolation of the data yields a value of 55.8 cal/g for the heat of fusion of 23.8 wt% U-Al alloy at the melting temperature of 640°C.

Experimental data on the heat of fusion of the alloy at temperatures above 640°C have not been found in the literature. An estimate of this quantity is obtained as follows: The heat necessary to melt a unit volume of uranium is about the same as that required for a unit volume of aluminum, or 250 cal/cm^3 [20]. Thus, for UAl_4, the density of which is equal to 5.7 g/cm^3 [26], the heat of fusion is about 43.9 cal/g, while for UAl_3, with density equal to 6.7 g/cm^3 [26], the heat of fusion is about 37.3 cal/g. Using these values, the energy absorption between 640 and 730°C is calculated to be 0.079 x 43.9 = 3.46 cal. At 730°C the energy absorption is 0.012 x 43.9 = 0.52 cal, and finally, the energy absorption between 730 and 960°C is 0.102 x 37.3 = 3.81 cal.

For digital calculational purposes, the small fraction of the alloy which melts at temperatures above 640°C was lumped with the large fraction of the alloy which melts at that temperature. In addition, the calculational assumption was made that the meat alloy melts in the temperature interval from 635 to 645°C, with a heat of fusion equal to the total heat absorbed in the temperature range from 640 to 940°C, or 63.6 cal/g. From Table A-IV, the density of the meat alloy at 640°C is about 3.09 g/cm^3. Thus, the value assumed for the volumetric heat capacity of the meat alloy during melting is

$$C(\text{cal/cm}^3\text{-°C}) = 3.09 \times 63.6 \times \frac{1}{10} = 19.7 \qquad \text{(A-17)}$$

For higher temperatures, the appropriate values for the volumetric heat capacity of the meat alloy were used (Table IV).

5.2 Heat of Fusion of Cladding and Melting Approximation

In the temperature range $622 \leq \theta \leq 649$°C, the type-6061 aluminum cladding melts, with an energy absorption of 94.5 cal/g. The density of the cladding at 622°C is about 2.65 g/cm^3. The volumetric heat capacity assumed for that temperature range was

$$C(\text{cal/cm}^3\text{-°C}) = 2.65 \times 94.5 \times \frac{1}{27} = 9.3 \qquad \text{(A-18)}$$

Above 649°C, the appropriate values for the volumetric heat capacity of 6061-aluminum were used (Table IV).